Wang C, Tremblay R, Rogers CA (2021), "Component-based model for bolted brace connections in conventional concentrically braced frames", Engineering Structures 247: 113137.

Component-Based Model for Bolted Brace Connections in Conventional Concentrically Braced Frames

Chen Wang[1], Robert Tremblay[2], Colin A. Rogers[3]

[1] Graduate Research Assistant, Department of Civil Engineering, McGill University, Montreal, QC, Canada.
Email: chen.wang5@mail.mcgill.ca

[2] Professor, Department of Civil, Geological and Mining Engineering, Polytechnique Montréal, Montreal, QC, Canada.
Email: robert.tremblay@polymtl.ca

[3] Corresponding author
Professor, Department of Civil Engineering, McGill University, Montreal, QC, Canada.
Email: colin.rogers@mcgill.ca
817 Sherbrooke Street West
Montreal, QC, Canada, H3A 0C3
Tel. 514 398-6449

Abstract

In low and moderate seismic regions, low-ductility concentrically braced frames (CBFs) are widely used as the seismic force-resisting system for steel structures. The capacity-based design method is not required for such systems, i.e. no individual component in the lateral load carrying path is explicitly designated to sustain plastic deformations under seismic loading. Such CBFs are referred to as conventional CBFs (CCBFs) in this paper. Prior studies have revealed that, in CCBFs, the brace-to-gusset connections are inherently weaker in tension than the adjoining braces and gusset plates. Therefore, the accurate numerical modelling of the brace connections is critical for the reliable seismic evaluation of CCBFs. However, few research publications address the inelastic bolted brace connection modelling necessary for the structural analyses of these braced frame systems. In this paper, an efficient inelastic numerical modelling method, comprising the component-based modelling concept, is proposed for bolted brace connections. The accuracy of the numerical model is validated through comparison with laboratory test results of full-scale I-shape brace connection specimens. Eight single-storey CCBFs with the symmetric diagonal bracing configuration were designed and modeled. The nonlinear static and dynamic analyses revealed that: 1) although the buckling of the middle column at small storey drifts resulted in substantial lateral strength deterioration, a secondary seismic mechanism provided stable resistance to prevent collapse; 2) when loaded in tension, the brace connections deformed more than the braces; 3) stronger brace connections resulted in higher structural lateral stiffness and triggered earlier buckling of the middle column; 4) stronger brace connections possessed higher frictional energy-dissipating capacity which reduced the maximum storey drift.

Keywords: low ductility, concentrically braced frame, bolted brace connection, component-based model, nonlinear dynamic analysis

1 Introduction

Concentrically braced frames (CBFs) are often used as seismic force-resisting systems because they are effective in providing structural lateral stiffness and strength. A variety of seismic design methods for CBFs with different levels of expected system ductility have been developed. In areas of low and moderate seismic hazard, low-ductility CBFs are permitted in many countries. Such CBFs are designed using a simple approach: the member forces are first calculated using linear elastic structural analysis; the structural members and connections are then designed to resist the obtained member forces. Capacity-based design and additional seismic detailing are not required. Such low-ductility CBFs are referred to as Conventional CBFs (CCBFs) in this study. Due to the expected low structural deformation capacity, CCBFs are typically designed for higher seismic loads as compared to more ductile lateral bracing systems.

Owing to the exemption for capacity-based design and additional seismic detailing, CCBFs are generally more economical than their more ductile counterparts. As such, CCBFs are widely used in low and moderate seismic regions in many countries. Each country may have its own designation and design requirements for the CCBF. In Canada, a low-ductility type of CBF, i.e. Type Conventional Construction (CC), is permitted as per CSA S16 [1]. Capacity-based design and seismic detailing are not required for structural members of Type CC CBFs, but the resistance of the brace connections must be increased by 1.5 if the expected connection failure mode is not proven to be ductile. In the USA, CBFs categorized as "Systems not specifically detailed for seismic resistance" in ASCE/SEI 7-16 [2] are prevalent in regions of low and moderate seismic hazard. To account for the modest expected structural deformation, a response modification factor, R=3, is assigned to such systems. In Europe, CBFs can be designed based on the concept of low dissipative structural behaviour with low structural ductility (DCL) per

Eurocode 8 [3]. Structural members and connections are simply required to resist the seismic loads calculated on the basis of an elastic global analysis, without any additional requirements. A behaviour factor (q) ranging from 1.5 to 2 is specified for design. In New Zealand, an elastic system with minimal structural displacement ductility demand (i.e. Category 4 system) is permitted in NZS 3404 [4]. A structural ductility factor (μ) of 1 is assigned. Furthermore, a performance factor (S_p) of 1.0 is specified for connections, compared to 0.9 for structural members, which effectively increases the design force demand on the connections.

In CCBFs, the brace-to-gusset connections tend to be inherently weaker than the adjoining braces and gusset plates. This is because, under the CCBF design framework, the brace-to-gusset connection, and the adjoining brace and gusset plate, are designed to resist the same forces. Braces and gusset plates are typically selected based on their respective compressive buckling resistances which are usually smaller than their respective tensile resistances, while brace-to-gusset connections are designed based on the tensile resistances. As such, both braces and gusset plates generally possess greater tensile resistances than the brace-to-gusset connections. This point has been verified both experimentally and numerically in prior studies. Sen et al. [5,6] experimentally studied CBFs that were built in the past without capacity-based design. Fracture of the brace-to-gusset welds was observed at low storey drifts. They concluded that the brace-to-gusset connection is of high priority in terms of retrofit of older CBFs. Bradley et al. [7] and Sizemore et al. [8,9] studied the seismic performance of low-ductility CBFs in the USA (including the R=3 CBFs) through full-scale system tests and numerical structural simulations. They found that the brace-to-gusset weld fracture was the dominant limit state; the as-built weld overstrength significantly affected the damage locations. To obtain insight into the seismic performance of CCBFs with I-shape braces and bolted brace connections, Rudman et al. [10] and

Wang et al. [11] conducted a series of full-scale tests of I-shape brace and bolted connection assemblies under reversed cyclic loadings. Wang et al. [12] subsequently developed high-fidelity finite element models to extend their experimental findings. Their studies revealed that significant plasticity and failure occurred in the brace-to-gusset connections when the specimens were loaded in tension, which confirmed that the bolted brace-to-gusset connection was weaker in tension than the adjoining braces and gusset plates.

Therefore, accurate modelling of the plastic behaviour and fracture of the brace connections is critical for the reliable seismic performance evaluation of CCBFs. Efforts have been taken to attain accurate brace connection modelling in previous studies. Hsiao et al. [13] developed a rotational spring model to account for the non-linear out-of-plane rotational restraint provided by brace connections. To account for the additional stiffness due to the presence of gusset plates, Qu et al. [14,15] modelled gusset plates as rigid, and added force-based fiber elements at the ends of braces to capture the rotational restraints. To represent the brace-to-gusset weld fracture, Hsiao et al. [16] implemented a translational spring at the brace end that had a linear-elastic response and a fracture displacement limit. In Sizemore et al. [8, 9], a translational spring was adopted to model the brace-to-gusset weld, and fracture was initiated based on a force limit. Moreover, in the modelling of their test frame, Sizemore et al. [8] used a gap-contact element to capture the reengagement between the brace and gusset plate after the brace-to-gusset weld fracture. Sen et al. [17] provided a framework for modelling welded gusset plate connections, in which the modelling of the gusset plate yielding, brace-to-gusset weld fracture, and gusset-plate interface weld fracture were covered. To model the bolted single shear lap connection, which are traditionally used for hollow structural section bracing members, Tremblay and Davaran [18] developed two OpenSees models. In the first model, the lap plates were modelled using the

beam-column elements individually, with truss elements with compression-only material placed between the lap plates to mimic the contact. In the second model, a single beam-column element with end plastic hinges was used for the entire connection.

However, it is noted that most previous studies on brace connection modelling were focused on welded brace connections. Limited research exists for the modelling of bolted brace connections. The high-fidelity continuum finite element analysis method could capture the bolted brace connection behaviour accurately, but such an approach is extremely computationally demanding and not practical for nonlinear dynamic structural analyses under earthquake loading, especially when extensive geometric and material nonlinearities are involved. There is a need to develop an accurate and computationally efficient numerical modelling method to capture the full behaviour range of bolted brace connections for reliable structural analyses of CCBFs.

The objective of this paper is to develop an accurate and efficient modelling method for bolted brace connections, specifically, the bolted flange plate brace connection. The component-based modelling concept was adopted in this study. This method first models each of the main components that constitute the brace connection, and then aggregates them as appropriate to reproduce the full behaviour of the connection. The ability of this method to characterize the force-deformation hysteretic behaviour and to predict the onset of fracture is then validated through comparison with experimental results. In the last section of this paper, the seismic performance of eight archetype buildings was evaluated through inelastic static (Pushover) analyses and Nonlinear Response History Analyses (NRHAs) with the brace connections modeled using the proposed component-based method.

2 Overview of the bolted flange plate brace connection

I-shape sections are widely used as the bracing members in CCBFs, as they are available with a wider range of sizes compared to other section types. Bolted connections are usually adopted to connect I-shape braces with other framing members, which avoids expensive on-site welding and expedites the construction process. A typical I-shape connection configuration is the flange plate connection shown in Figure 1.

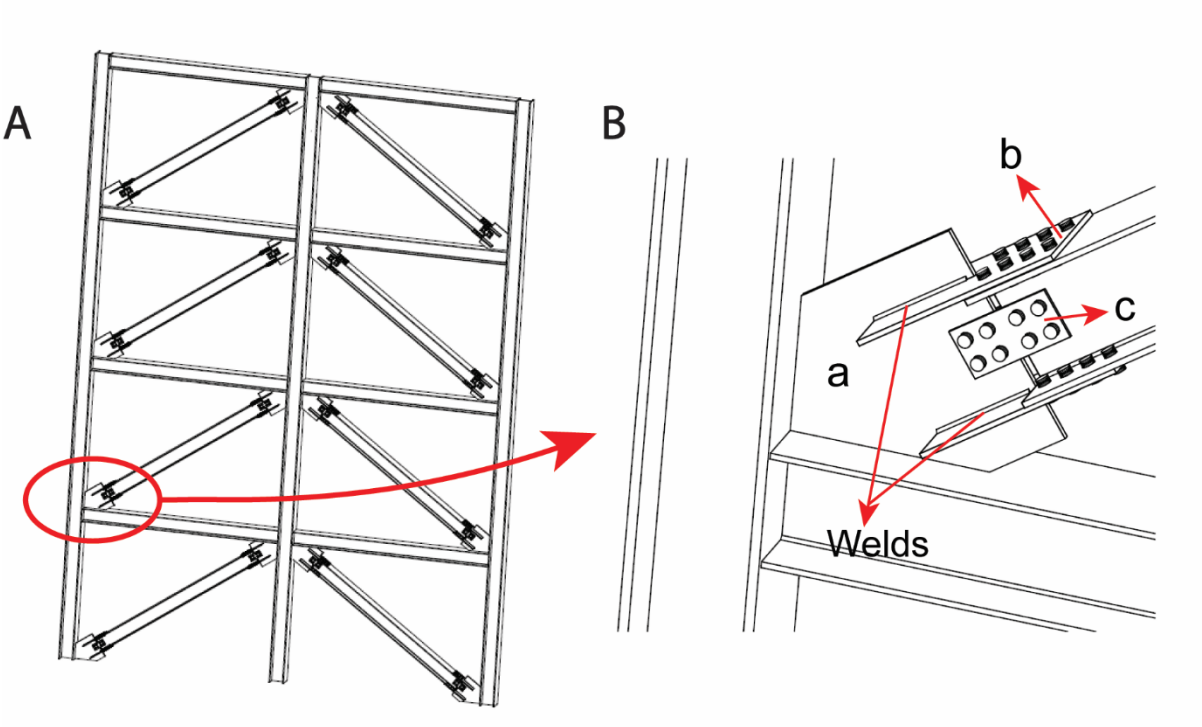

Figure 1 Schematic of CCBF with I-shape braces and flange plate brace connection: a) gusset plate, b) flange lap plate (FLP), c) web lap plate (WLP)

The behaviour of the flange plate brace connection was evaluated in previous studies both experimentally [10,11] and numerically [12]. The force transfer mechanism under reversed cyclic loading was characterized, and the force flow path through individual components of the flange plate connection was identified (Figure 2).

In this paper, the flange plate brace connection is used to illustrate the implementation of the component-based modelling method to construct numerical models for bolted brace connections; the experimental results serve the validation of the method.

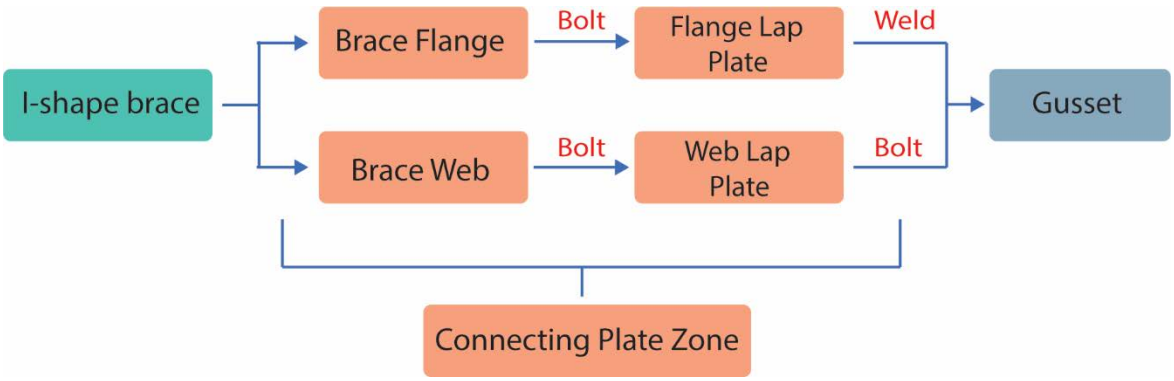

Figure 2 Components and force paths of the flange plate brace connection

3 Component-based brace connection modelling method

The component-based modelling concept provides a flexible numerical framework to model the response of complex connections, especially when there is no general model available to capture the full-range of behaviour of the connection [19,20]. Rather than attempting to extract one general model for the whole connection, the component-based method discretizes the connection into individual components that contribute to the global behaviour. Each component is modeled by a spring with the characteristic behavioural properties; the interactions between the components are captured by arranging springs either in parallel or in series, as appropriate.

There is no prescribed yielding/failure hierarchy in the bolted flange plate brace connection in CCBFs, as explained by Wang et al. [12]; therefore, any one of the components illustrated in Figure 2 could dominate the behaviour, and should be incorporated in the numerical model. For the multi-bolted component, e.g. the bolted flange lap plate, it is further discretized into

individual single-bolted components, which comprise a bolt and two bearing plates (Figure 3), as utilized by Weigand [21]. The description and modelling of individual components involved in the flange plate connection are elaborated in the following sections. Note that the component-based method is not limited to the flange plate brace connection, it can easily be extended to other bolted brace connection configurations based on the same philosophy, by changing the constituting components, as appropriate.

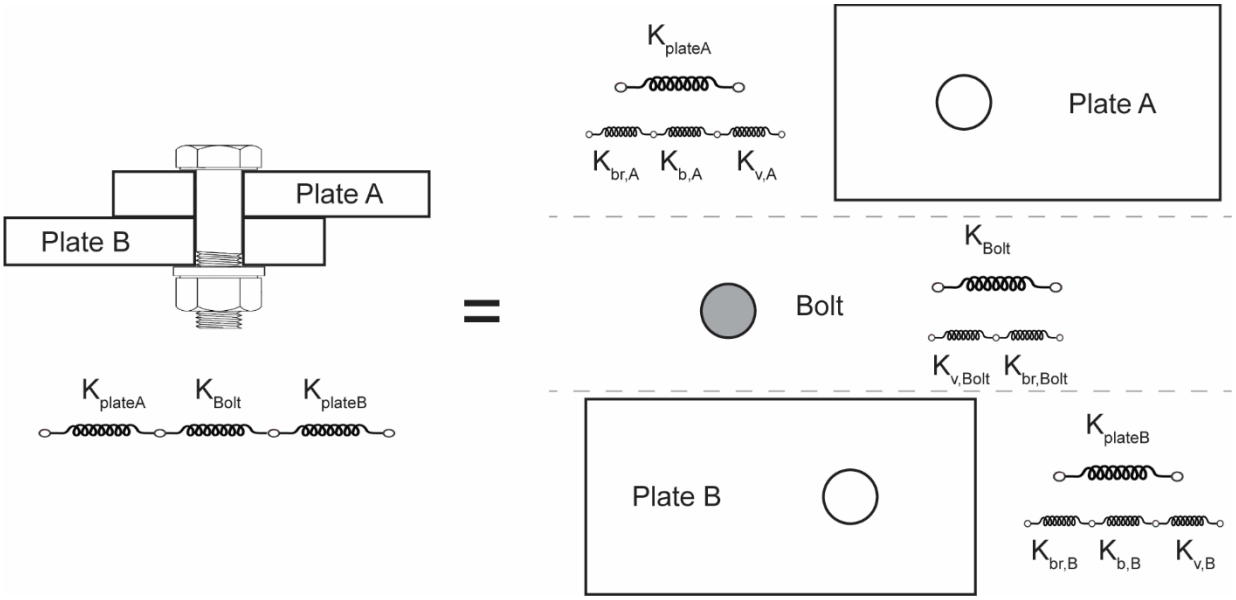

Figure 3 Disaggregation of the single-bolted component

3.1 Bearing Behaviour

The bearing behaviour of the plate was analytically established by Rex and Easterling [22], who performed 46 tests of a single bolt bearing against a single plate with various edge distances, plate thicknesses, bolt diameters, plate widths, and edge conditions. They adopted the equation proposed by Richard and Abbott [23], commonly known as the Richard equation, and calibrated

the equation parameters based on their experimental results using a nonlinear least-square regression technique. The load-deformation relationship in bearing is:

$$\frac{\mathrm{R}}{\mathrm{R_n}} = \frac{(\alpha_{kb} - \alpha_{kp})\overline{\Delta}}{\left[1 + \left|\frac{(\alpha_{kb} - \alpha_{kp})\overline{\Delta}}{\alpha_{rb}}\right|^{n}\right]^{\frac{1}{n}}} + \alpha_{kp}\overline{\Delta} = \frac{1.74\overline{\Delta}}{\left(1 + \overline{\Delta}^{\frac{1}{2}}\right)^{2}} - 0.009\overline{\Delta} \quad (1)$$

where R = bearing load, R_n= plate ultimate bearing strength, $\overline{\Delta}$ = normalized bearing deformation, with $\alpha_{kb} = 1.731$, $\alpha_{kp} = -0.009$, $\alpha_{rb} = 1.740$, and $n = 0.5$.

There are several limits available in different standards in terms of the ultimate plate bearing strength. The model for predicting the plate ultimate bearing/tearing strength (F_b) developed by Fisher and Struik [24] was adopted in this study:

$$F_b = 1.4F_u\left(\frac{L_e}{d_b} - \frac{1}{2}\right) \leq 3.0F_u \quad (2)$$

where F_u = ultimate stress of the steel material, L_e = end distance of the bolt, d_b = bolt diameter.

The normalized deformation $\overline{\Delta}$ is equal to $\Delta\beta K_i/R_n$, where Δ = hole elongation, β = steel correction factor (taken as one for typical steels), K_i = initial stiffness. Through experimental tests and numerical simulations Rex and Easterling [22] found the initial stiffness depended on three primary stiffness mechanisms in the plate—bearing, bending, and shearing. The model that accounts for these three stiffnesses is:

$$K_i = \frac{1}{\frac{1}{K_{br}} + \frac{1}{K_b} + \frac{1}{K_v}} \quad (3)$$

where K_{br} = bearing stiffness, K_b = bending stiffness, K_v = shearing stiffness, and they are quantified as:

$$K_{br} = 120 t_p F_y \left(\frac{d_b}{25.4}\right)^{0.8} \tag{4}$$

$$K_b = 32 E t_p \left(\frac{L_e}{d_b} - \frac{1}{2}\right)^3 \tag{5}$$

$$K_v = 6.67 G t_p \left(\frac{L_e}{d_b} - \frac{1}{2}\right) \tag{6}$$

with t_p = thickness of the plate.

3.2 Bolt behaviour

The shear force-deformation behaviour of the bolt can also be described by means of the Richard equation, as done by Weigand [21]:

$$R_{bolt} = \frac{\left(K_{i,bolt} - K_{p,bolt}\right)\Delta}{\left[1 + \left|\frac{\left(K_{i,bolt} - K_{p,bolt}\right)\Delta}{R_{v,bolt}}\right|^2\right]^{\frac{1}{2}}} + K_{p,bolt}\Delta \tag{7}$$

where R_{bolt} = shear force, Δ = shear deformation, $K_{i,bolt}$ = bolt initial stiffness, $K_{p,bolt}$ = bolt plastic stiffness, and $R_{v,bolt}$ = bolt shear capacity.

The initial stiffness of the bolt, $K_{i,bolt}$, is primarily affected by bearing and shearing in the bolt shank, and therefore is calculated by assuming two springs in series as:

$$K_{i,bolt} = \frac{1}{\frac{1}{K_{br,bolt}} + \frac{1}{K_{v,bolt}}} \tag{8}$$

where $K_{br,bolt}$ = bolt bearing stiffness and $K_{v,bolt}$ = bolt shearing stiffness.

Nelson et al. [25] proposed a model for bolt bearing stiffness based on their experimental work,

$$K_{br,bolt} = \frac{1}{1 + 3\beta_b} \frac{t_p t_w E_{bolt}}{2(t_p + t_w)} \tag{9}$$

where t_w is the thicknesses of the connected plate, and β_b is a correction factor that represents the fraction of the total bending moment on the bolt that is reacted by the nonuniform bearing stresses across the thickness of the connected plate. Many factors may affect the value of β_b, e.g., the bolt geometry and bolt pretension, the size of nuts and washers, the ratio of bolt diameter to plate thickness, among others. The value of β_b could vary from a maximum of 1.0 for simple shear pin, to a very small value for bolted connections with large washers and a large ratio of bolt diameter to plate thickness. It is worth noting that limited data are available to calibrate the value of β_b for bolted joints in steel structures. A value of β_b = 0.7 was adopted by Weigand [21] in models for 13 steel shear connections, in which bolts of two grades (A325 and A490) and various diameters (19-22 mm) were used. Good agreement between the predicted connection stiffness with the experimental ones reported in Weigand and Berman [26] was obtained. In this study, the same bolt grades (A325 and A490) and similar bolt diameters (16-20 mm) were used, and the same value of β_b = 0.7 was adopted.

The bolt shearing stiffness is determined by assuming that the bolt acts as a prismatic Timoshenko beam with circular cross section and fixed ends,

$$K_{v,bolt} = \frac{12E_{bolt}I_{bolt}}{L_{bolt}^3(1+\Phi)} \quad (10)$$

where E_{bolt} = bolt modulus of elasticity, $I_{bolt} = \frac{\pi d_b^4}{64}$ = moment of inertia of the bolt shaft cross section, $L_{bolt} = t_p + t_w$ = bolt length, and

$$\Phi = \frac{12E_{bolt}I_{bolt}}{G_{bolt}\kappa A_{bolt}L_{bolt}^2} \quad (11)$$

is a term that accounts for the relative importance of shear deformation to bending deformation in Timoshenko beam theory [27]. In equation (11), $G_{bolt} = \frac{E}{2(1+\nu)}$ is the bolt shear modulus, A_{bolt} is the bolt cross section area, and κ is the shear coefficient for a circular cross section

$$\kappa = \frac{1}{\frac{7}{6} + \frac{1}{6}\left(\frac{\nu}{1+\nu}\right)^2} \quad (12)$$

Based on the bolt shear test data [28], the bolt shear capacity was taken as

$$R_{v,bolt} = 0.62A_{bolt}F_{u,bolt} \quad (13)$$

and the bolt plastic stiffness $K_{p,bolt}$ was calculated as 2% of the bolt initial stiffness $K_{i,bolt}$.

3.3 Weld behaviour

In the bolted flange plate brace connection, the flange lap plates (FLPs) are connected to the gusset plate by fillet welds that are parallel to the line of action of the brace force (Figure 1). The expression developed by Lesik and Kennedy [29] for load-deformation response of welds loaded longitudinally, i.e. at an angle of 0º, was therefore adopted:

$$P = P_0 f(\rho) \tag{14}$$

where P_0 is the ultimate strength of the longitudinal weld. The function $f(\rho)$ gives the variation of load with respect to deformation, and is defined as:

$$\begin{aligned} f(\rho) &= 8.234\rho; \qquad 0 < \rho < 0.0325 \\ f(\rho) &= -13.29\rho + 457.32\rho^{\frac{1}{2}} - 3385.9\rho^{\frac{1}{3}} + 9054.29\rho^{\frac{1}{4}} - 9952.13\rho^{\frac{1}{5}} \\ &\quad + 3840.71\rho^{\frac{1}{6}}; \quad \rho > 0.0325 \end{aligned} \tag{15}$$

In equation (15), ρ is the normalized deformation with respect to the deformation at ultimate strength,

$$\rho = \frac{\Delta}{\Delta_u} = \frac{\Delta}{0.209 \times 2^{-0.32D}} \tag{16}$$

where Δ and D are the weld deformation and fillet weld size in the same units, respectively.

By using the weld resistance equation in Clause 13.13.2.2 of CSA S16 [1], the ultimate strength of a longitudinally loaded weld is calculated as

$$P_0 = 0.67\phi A_W X_u \tag{17}$$

where A_W is the effective throat area of the fillet weld, X_u is the ultimate strength of the weld metal, and the resistance factor ϕ was taken as one to obtain a realistic estimate of the strength.

3.4 Brace connection modelling in OpenSees

The component-based brace connection modelling was implemented in OpenSees [30]. The spring model structure for the flange plate brace connection, with each spring representing one constituting component of the connection, is schematically shown in Figure 4.

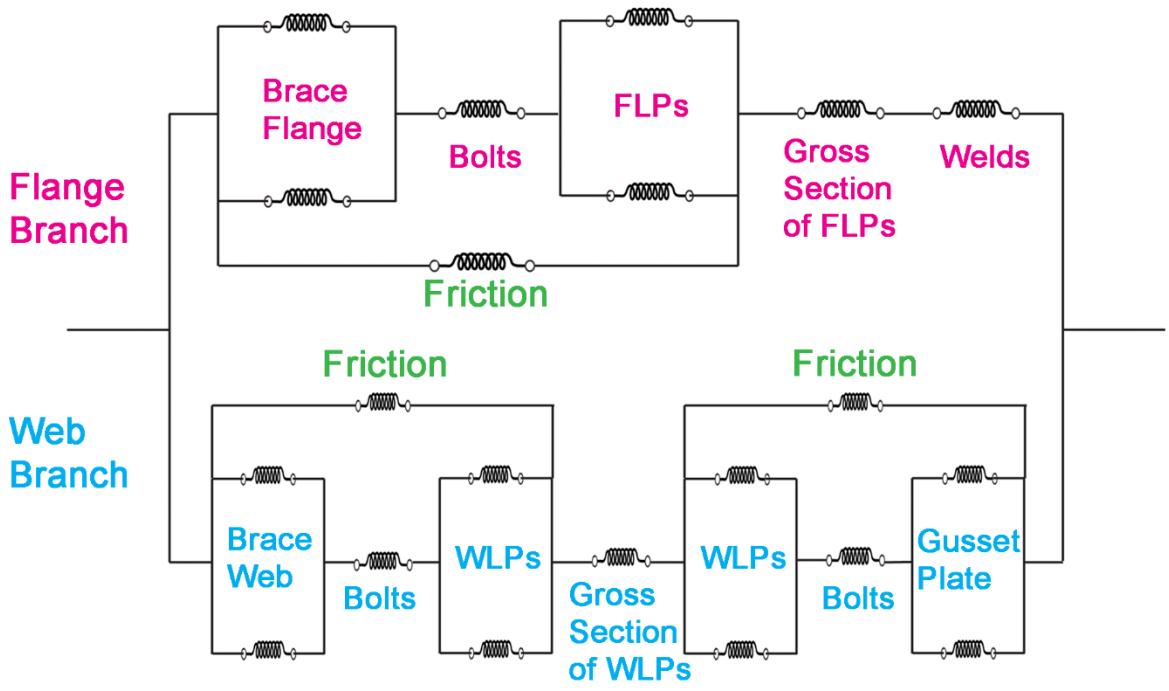

Figure 4 Spring model structure of the bolted flange plate brace connection in OpenSees

Bolt slippage plays a significant role in the cyclic response of bolted brace connections. In order to capture the pronounced bolt slippage behaviour, a pair of Elastic-Perfectly Plastic Gap (EPPG) elements were selected for each bearing component, with one for tensile bearing and the other for compressive bearing behaviour. Before the specified gap is taken up, the EPPG element provides zero resistance. It was assumed that the bolt hole diameter was 1.6 mm (1/16 in.) greater than the bolt diameter, and all the bolts were initially in the middle of the bolt holes. As

such, the initial gap values were set as 0.8 mm and -0.8 mm for the tensile bearing element and the compressive bearing element, respectively. Moreover, for each gap element, the 'damage' option was turned on so that the gap value would grow with the plastic deformation of the bolt hole to account for the bolt hole elongation phenomenon. Frictional forces were reported to decrease upon cyclic loading [10,11]; at the final phase of the tests, a mean value of 17% was obtained for the ratio of the frictional force to the force based on which the brace connection was designed. In the OpenSees model, the friction was modelled by placing an Elastic-Perfectly Plastic (EPP) element parallel to the EPPG elements, with the frictional force set equal to 17% of the force based on which the brace connection was designed. The bearing behaviour after the gap was closed was determined by the analytical method described in Section 3.1, and simplified as bilinear with the ratio of post-yield stiffness to initial stiffness set as 0.04. The bolt and weld behaviours were modelled using the Steel02 material in OpenSees [31]. The Steel02 material parameters were determined to make the backbone curve of the force-deformation hysteretic loops match with the response curve predicted in accordance with the equations in Section 3.2 and Section 3.3: R0=4, cR1=0.01 and cR2=0.01 for bolts, and R0=3, cR1=0.01 and cR2=0.01 for welds. Figure 5 shows a comparison between the behaviours predicted by the equations and the response provided by the OpenSees model for typical components of the tested specimen J310-T by Rudman et al. [10]. They are representative of the simulation of tensile bearing behaviour, cyclic bolt shear behaviour, and cyclic weld behaviour.

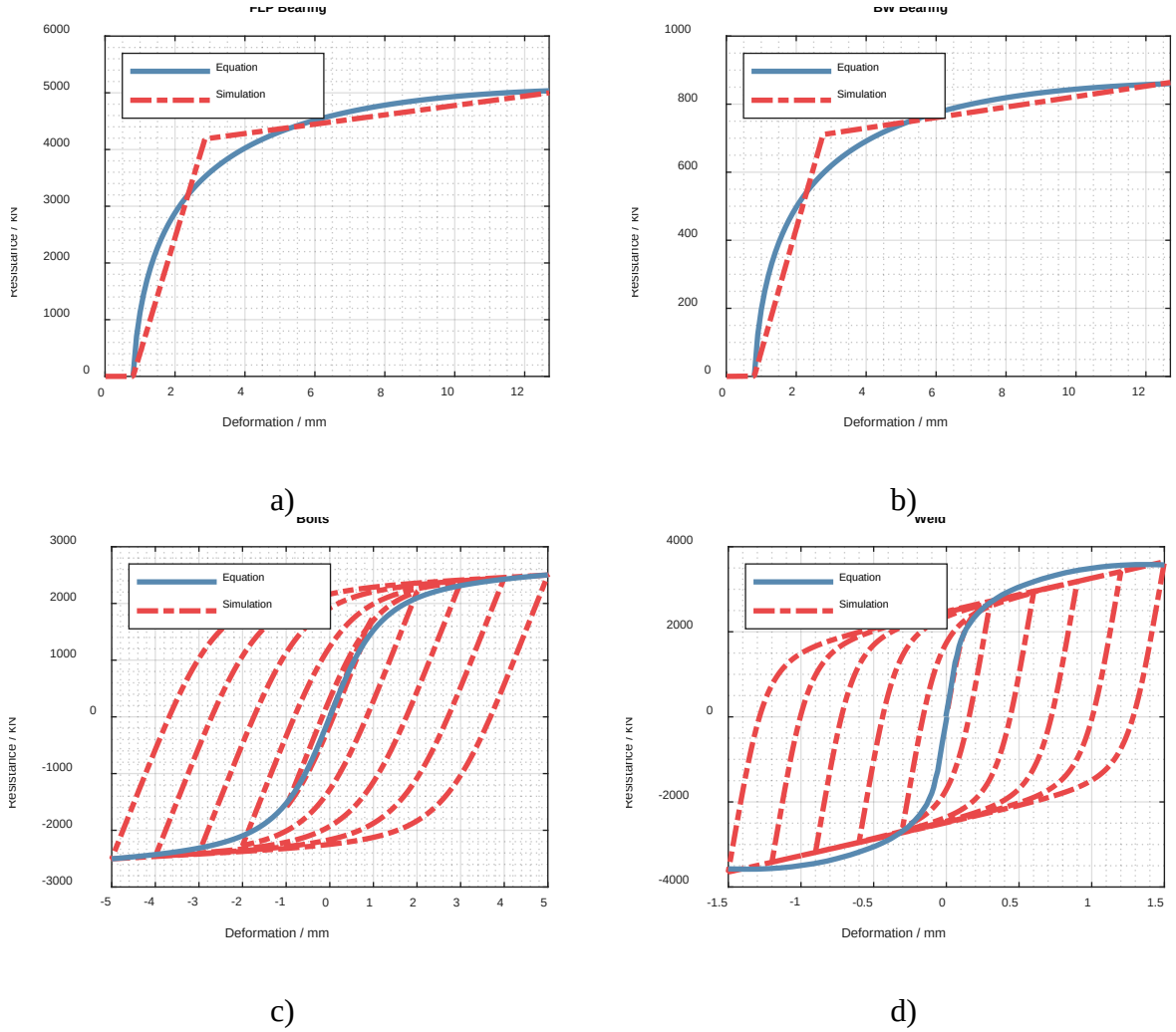

Figure 5 Comparison of simulated and numerically predicted behaviour of typical components: a) FLP bearing, b) Brace web bearing, c) Bolts in the brace flange, and d) Welds

3.5 Fracture criteria

To capture the fracture that could be caused by various mechanisms, fracture criteria were introduced to individual components in the OpenSees model. The bolt shear tests reported by Wallaert & Fisher [32] and Weigand [28] indicated that the high-strength bolt (e.g., grade A325 and A490 bolts) generally failed in shear at 5 mm (0.2 in.) deformation, which was selected as the bolt deformation limit. The MinMax material in OpenSees was adopted to introduce the

maximum deformation limit. If the deformation fell above the prescribed limit, the element was assumed to have failed and values of zero were returned for the stiffness and strength.

Likewise, fillet welds loaded longitudinally were reported to reach their ultimate strength at a deformation approaching 0.2D (D is the fillet weld size), after which they lost their strength quickly [29]. In the model, the weld deformation limit was set to 0.2D. The plate bearing failure was defined when the bearing deformation exceeded 12.7 mm (0.5 in.), as done by Rex and Easterling [22]. In some cases, fracture may occur along the net section of the FLPs and WLPs. In view of the limited deformation capacity associated with net section fracture, the force-based limit was set to model the net section fracture, with the value determined by:

$$T_u = A_n R_t F_u \tag{18}$$

where A_n = area of net section, R_t = the ratio of the expected tensile ultimate strength to the minimum tensile ultimate strength of the steel.

3.6 Validation

To verify the validity of the component-based brace connection modelling method, numerical models were built in OpenSees for the tested full-scale brace-connection assemblies reported in Rudman et al. [10] and Wang et al. [11]. Knowing that the numerical models described herein were not developed to capture gusset plate buckling, only the test specimens that exhibited brace buckling in compression were modeled, specifically specimens J-310-C and J-310-T in Rudman et al. [10] and specimen J360-P in Wang et al. [11].

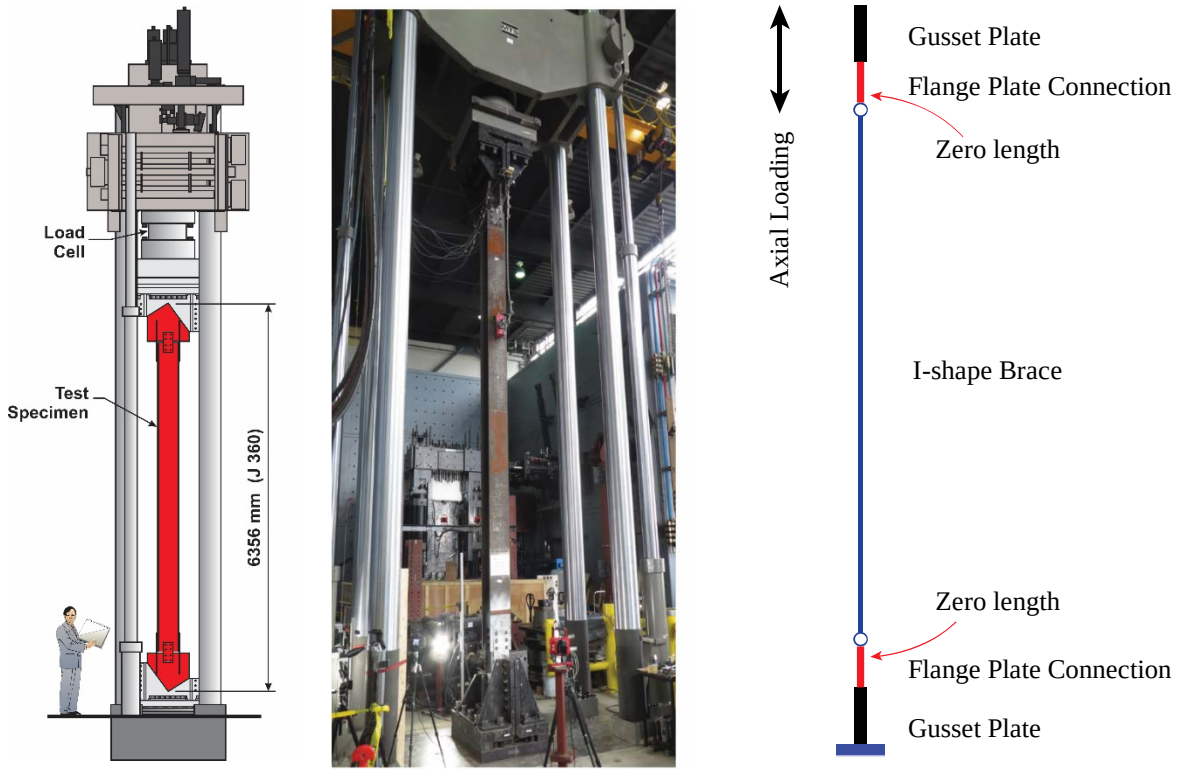

Figure 6 Modelling of tested full-scale brace-connection assemblies in OpenSees: a) test set-up [10,11]; b) OpenSees model

As shown in Figure 6, the tested specimens contained three parts: gusset plates, flange plate connections, and I-shape brace. The flange plate connections were modeled following the approach in Section 3.4, and the modelling parameters of each component were calculated based on the measured geometric and material properties [10,11]. For each brace, ten displacement-based beam-column elements with five integration points in each element were used. The fiber-based section, with 10 fibers along flange width/web height and 4 fibers through flange thickness/web thickness, was assigned to each element. This discretization scheme is slightly more stringent than that recommended by Karamanci & Lignos [33]. An initial out-of-straightness of 1/1000 times brace length following a half sine wave distribution was introduced. Due to the configuration of the flange plate brace connection, the end rotation restraint about the

I-shape brace minor axis is far smaller than that about its major axis. As such, the initial out-of-straightness was only introduced for the minor axis of the I-shape braces because they were expected to buckle about this axis. The brace was pin connected to the gusset plate through the flange plate connection. The Steel02 material was used for braces, with the yield strength, initial elastic tangent, and strain-hardening ratio (b=0.29%) determined based on the tension coupon test results reported in Rudman [34]. Other parameters in the model were R0=15, cR1=0.925, and cR2=0.15 as recommended in Mazzoni et al. [35]. Previous research has been conducted to capture the low-cycle fatigue rupture behaviour [15,36]. However, due to the fact that in CCBFs braces are not expected to experience low-cycle fatigue rupture, this failure mode was not modelled in this study.

In CCBFs with I-shape braces and bolted brace connections, the bolted brace-to-gusset connection is weaker than the adjoining brace and gusset plate, especially when loaded under tension. This is because, under the non-capacity design framework, the brace-to-gusset connection, and the adjoining brace and gusset plate, are designed to resist the same force demand calculated through elastic structural analysis. Braces and gusset plates are typically selected and designed based on their respective compressive buckling resistances, which are usually smaller than their respective tensile resistances. However, brace-to-gusset connections are typically designed based on their tensile resistances, as compressive buckling is not expected to occur in the connections. As such, when loaded under tension, the brace-to-gusset connection is weaker than the adjoining brace and gusset plate; plastic deformations leading to failure are expected to occur in the brace-to-gusset connection rather than in the gusset plate. This has been verified experimentally through full-scale tests of brace and bolted brace connection assemblies by Rudman et al. [10] and Wang et al. [11], and numerically by Wang et al. [12,37]. Therefore,

the gusset plates were modelled as rigid bodies in this study, by using a displacement-based beam-column element assigned with a very large section (more than 1000 times larger than the brace section) and the brace material.

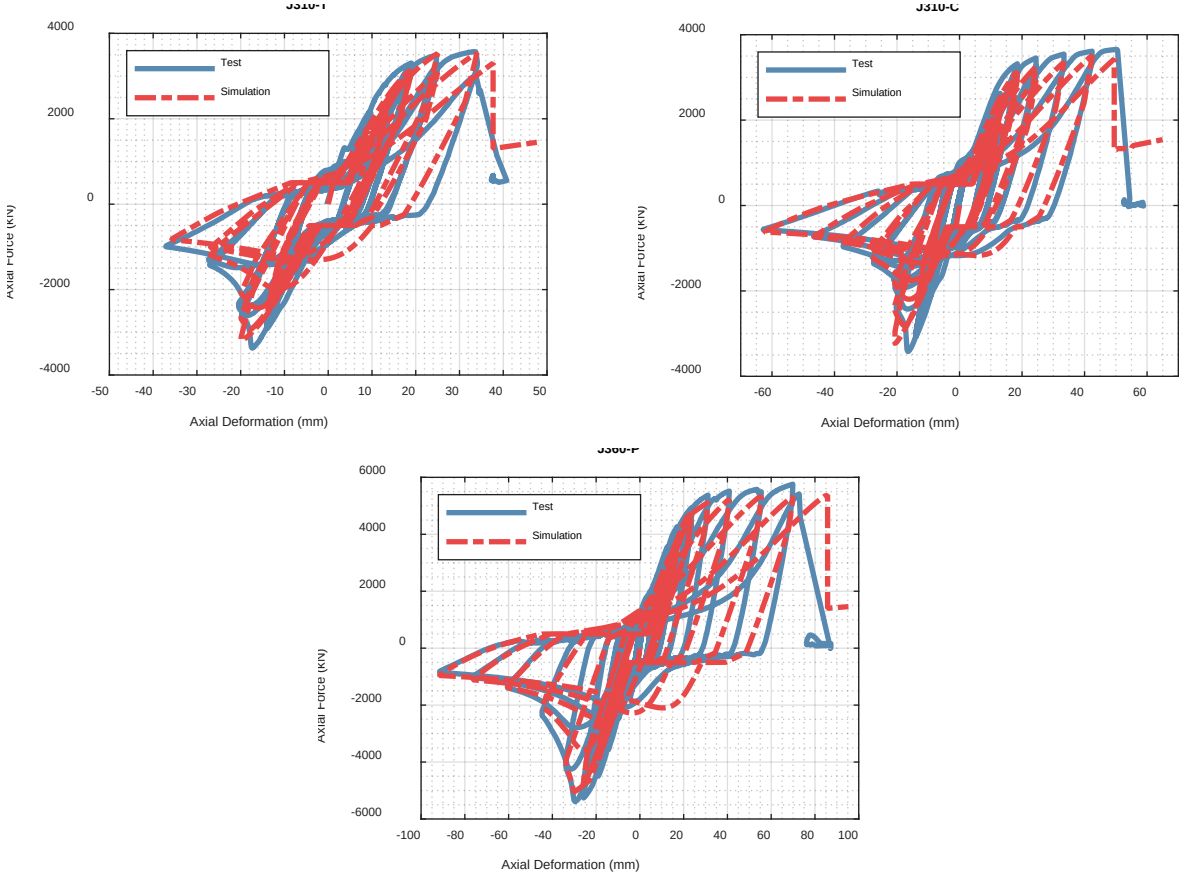

Figure 7 Comparison of simulated and experimental [10] axial force-deformation responses of the brace-connection assembly

Reversed cyclic loading was simulated following the loading protocols used in the laboratory tests [10,11]. The axial force-deformation results obtained from the numerical simulations were compared with those acquired from the tests [10,11], as shown in Figure 7. These force-deformation hysteretic curves exhibited good agreement, and the numerical models accurately predicted the connection failure mode (bolt shear rupture) at similar deformation levels to those

reported in the tests, indicating the capability of the proposed component-based brace connection modelling method to capture the cyclic behaviour and failure of the connections.

In addition, the brace connection axial deformation histories at one end of the brace, excluding the brace axial deformation, were extracted from the numerical simulations and compared with those measured during the tests [10,11], as shown in Figure 8. A generally good match was obtained, which further validated the accuracy of the component-based brace connection model.

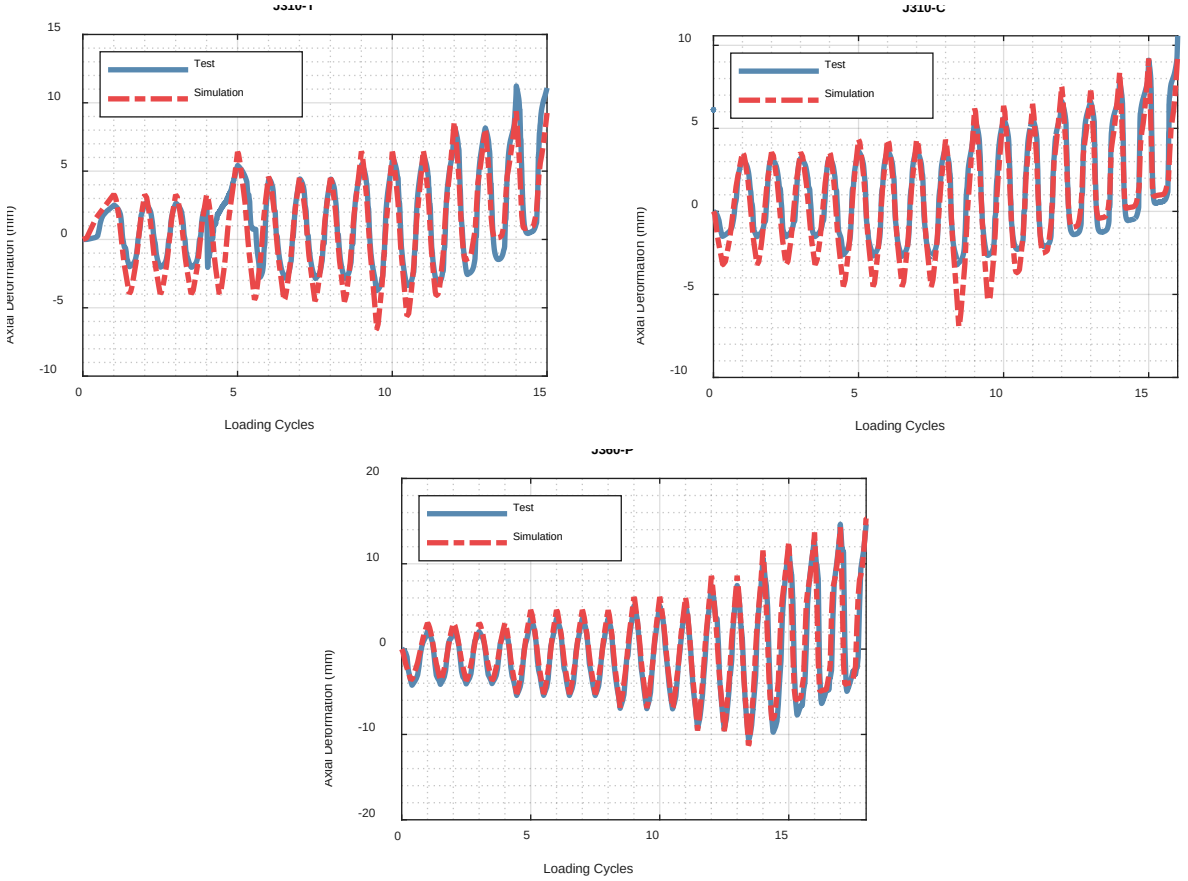

Figure 8 Comparison of simulated and experimental [10,11] axial deformation histories of one brace connection

3.7 Significance of modelling bolted brace connections

The deformation histories of the brace connections at the both ends of the brace, the brace, and the entire specimen, for the three validation models, are compared in Figure 9. Before brace buckling occurred, most deformation developed in the brace connections under both tension and compression loadings. After brace buckling had occurred, due to the sudden degradation of the brace compressive resistance, most deformation concentrated in the brace under compression loading; however, when loaded under tension loading, the deformation from the brace connections still constituted a significant portion of the total deformation. For all three specimens, ultimate failure occurred in the brace connections.

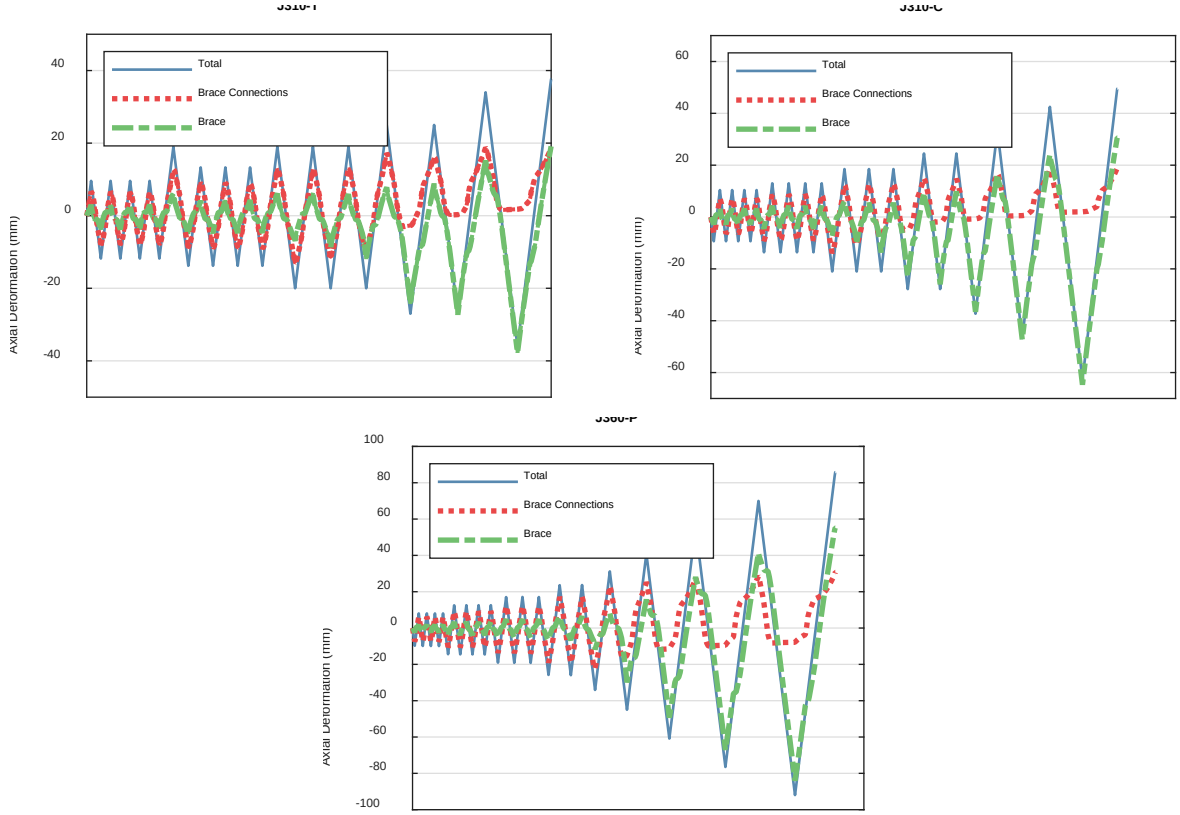

Figure 9 Comparison of deformation histories between brace and brace connections

Moreover, simulations were conducted in which the brace connections were not modelled, while all the other aspects (other elements, boundary conditions, loading protocols, etc.) were maintained. In Figure 10, the force-deformation hysteretic response results are compared between the models with and without the brace connections.

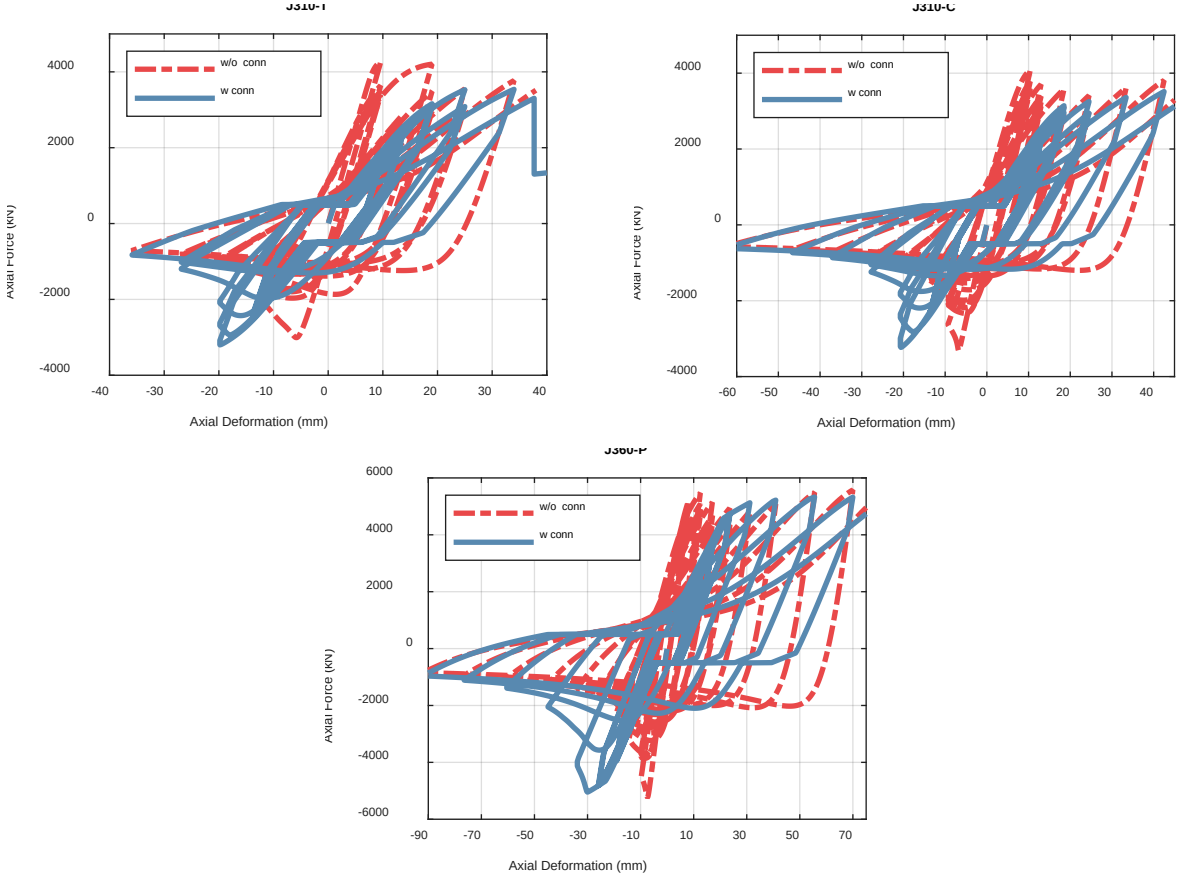

Figure 10 Response comparison between models with (w) and without (w/o) the brace connections

The behaviour of the bolted brace connections significantly affected the response of the brace and brace connection assembly. Firstly, the axial stiffness of the assembly was noticeably reduced with the incorporation of the brace connections. Secondly, as explained in Section 3.6, the tensile strength of the assembly was usually controlled by the tensile strength of the brace connections in CCBFs. Without modelling the brace connections, the tensile strength of the

brace controlled, which resulted in a greater tensile strength for the assembly. Thirdly, significant axial deformation occurred in the bolted brace connections, including slip, bolt hole elongation, and deformation of other components, which substantially affected the force-deformation hysteresis of the assembly. When loaded under compression, the abrupt strength loss due to brace buckling occurred at a much larger deformation level when the brace connections were modeled. When loaded under tension, the assemblies developed much higher strength at small deformation levels when the brace connection deformation was not accounted for. Moreover, whenever the load was reversed, the slip in the bolted brace connections, which increased in magnitude over the course of the loading protocol due to bolt hole elongation, resulted in a plateau in the axial force-deformation response and pinched hysteresis loops. This was not captured when the brace connections were not modelled.

4 Case study

To study the effect of brace connection behaviour on the seismic response of CCBFs, eight archetype buildings located in areas of different seismic hazard levels in Canada were designed and analyzed. Two brace connection strength levels and two beam orientations were considered. The validated component-based modelling approach described in Section 3 was adopted for all the brace connection modelling in the analyses.

4.1 Archetype building design

Eight single-storey buildings with CCBF seismic systems were designed. The building dimensions and building plans with different beam orientations are shown in Figure 11. A two-bay symmetric diagonal bracing configuration, with braces connected at the top end of the middle column, was adopted for the CCBF. For one-storey CCBFs with such bracing

configuration, the braces will not impose large forces on other structural members under the elastic structural response, and economical design can usually be achieved. Loading was applied to the buildings in the EW direction. They are located either on a site class E (soft soil) in Vancouver, BC, representing regions of high seismic hazard, or on a site class C (firm ground) in Montreal, QC, representing regions of moderate seismic hazard. Other design parameters including loads, load combinations, and structural materials, are listed in Table 1.

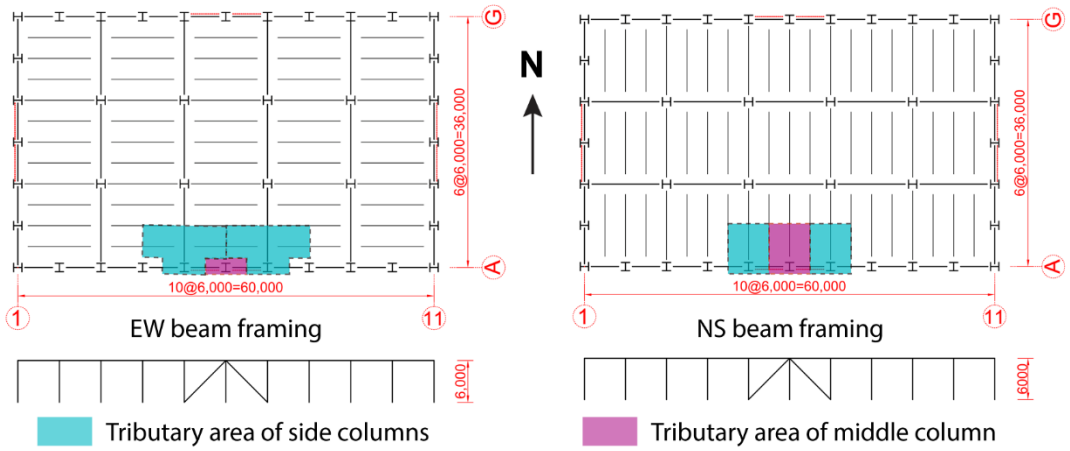

Figure 11 Building plans with different secondary beam orientations (dimensions in mm)

Table 1 Building design parameters

Loads	Roof dead load: 0.98 kPa Roof live load: 1 kPa Wall: 4.94 kPa Snow load: 1.64 kPa (Vancouver) and 2.48 kPa (Montreal)
Load combinations	1.4D 1.25D+1.5L+1.0S 1.25D+1.0L+1.5S 1.0 E+1.0D+0.5L+0.25S
Structural materials	W sections: A572 Grade 50 Plates: A572 Grade 50 Bolts: A490/A325 Welds: E49

The CCBFs were designed following the Equivalent Lateral Force Procedure with the design base shear calculated as per the National Building Code of Canada (NBCC) [38]. The required strengths for structural components and connections were subsequently determined through a linear elastic structural analysis without consideration of the capacity-based design principle. The two adjacent braces were assumed to equally resist the seismic load and their contribution to resist gravity loads was not considered. It is worth mentioning that the unbalanced force resulting from brace buckling was not accounted for in the linear elastic structural analysis. The columns (both the middle column and side columns) were only designed to carry gravity loads. The orientation of the secondary beams in the East-West direction (referred to as the EW orientation) resulted in a larger tributary area for the middle column and a smaller tributary area for the side columns compared to the NS orientation (Figure 11), which resulted in stronger middle columns and weaker side columns (EW orientation).

Table 2 Studied archetype buildings and design of CCBFs

CCBF ID	Location	Site Class	Secondary Beam Orientation	Brace Connection Strengthening (%)	Brace	Beam	Middle Column	Side Column
VE-EW-100	Vancouver	E	EW	100	W250×73	W310×28	W150×18	W200×36
VE-EW-150	Vancouver	E	EW	150	W250×73	W310×28	W150×18	W200×36
VE-NS-100	Vancouver	E	NS	100	W250×73	W360×33	W130×28	W130×28
VE-NS-150	Vancouver	E	NS	150	W250×73	W360×33	W130×28	W130×28
MC-EW-100	Montreal	C	EW	100	W200×52	W250×18	W100×19	W200×42
MC-EW-150	Montreal	C	EW	150	W200×52	W250×18	W100×19	W200×42
MC-NS-100	Montreal	C	NS	100	W200×52	W360×33	W150×30	W150×30
MC-NS-150	Montreal	C	NS	150	W200×52	W360×33	W150×30	W150×30

The archetype building matrix and the design results of CCBFs are listed in Table 2. With regard to the CCBF ID, the first term indicates the location and site class of the building, with VE meaning Vancouver and site class E, and MC meaning Montreal and site class C; the second

term denotes the secondary beam orientation; and the last term represents different brace connection designs, which will be described further in the next section.

4.2 Brace connection design

Two brace connection designs were studied: one based on the seismic force demand obtained through the linear elastic structural analysis, the other based on the force demand amplified by 1.5. Such variation was intended to evaluate the different specifications for the brace connection design force in different seismic codes. In the USA and Europe, there is no seismic design force amplification requirement for brace connections in CCBFs (i.e. the R=3 CBF in ASCE/SEI 7-16 [2] and the DCL CBF in Eurocode 8 [3]). In contrast, in Canada, the seismic design forces of brace connections are required to be amplified by 150% for CCBFs (i.e. the Type CC CBF in CSA S16 [1]), if the brace connections are not shown to be ductile. In the CCBF ID listed in Table 2, the terms “100” and “150” indicate the brace connection designs based on the normal force demand (i.e. 100%) and the 1.5-times amplified force demand (i.e. 150%), respectively.

Table 3 Design of brace connections

CCBF ID	Design Force (kN)	Bolt				FLP		WLP		Gusset		Weld	
		Grade	Size	n_F	n_W	t	w	t	w	t	w*	D	L
VE-EW-100	974	A490	16	8	2	12	150	10	110	10	392	8	100
VE-NS-100	974	A490	16	8	2	12	150	10	110	10	392	8	100
MC-EW-100	427	A325	20	4	1	10	120	10	60	8	295	6	60
MC-NS-100	427	A325	20	4	1	10	120	10	60	8	295	6	60

Note: dimensions in mm; n_F = number of bolts in the flange branch; n_W = number of bolts in the web branch; t = thickness; w = width; D = fillet weld size; L = weld length
*Whitmore width

As shown in Figure 2, the flange plate brace connection consists of two force paths, namely, the flange branch and the web branch. In design practice, engineers usually assume that the ratio of

the force in the flanges to the force in the web is equal to the ratio of the brace flange area to the brace web area. This assumption was adopted in the brace connection design in this study to allow the design to match the procedures commonly used in practice. The design results of the brace connections that were designed based on the non-amplified design forces are listed in Table 3. The modelling of the brace connections that were designed based on the 1.5-times amplified design forces was achieved by multiplying the stiffnesses and strengths of the corresponding non-strengthened ones by 1.5.

4.3 OpenSees modelling of CBFs

All studied CCBFs were modeled in OpenSees (Figure 12). Both the in-plane and out-of-plane degrees of freedom were considered for all nodes to account for the possible out-of-plane deformation of structural members. The braces, brace connections and gusset plates were modelled following the validated approach described in Sections 3.4 to 3.6. The expected material strengths (the expected yield strength, R_yF_y, and the expected tensile strength, R_tF_u) calculated as per AISC 341-16 [39], were used to define the material properties and to calculate the material related parameters. Similar to the modelling of the braces, the beams and columns were also modeled using ten displacement-based beam-column elements with five Integration Points. The fiber-based section, with 10 fibers along the flange width/web height and 4 fibers through the flange thickness/web thickness, was assigned to each element. The Steel02 material was used for the braces, beams and columns, with the same parameters as those specified in Section 3.6, except that the yield strength was set as the expected yield strength (R_yF_y) calculated in accordance with AISC 341-16 [39]. For the columns, an initial out-of-straightness imperfection of 1/1000 the member length following a half sine wave distribution was introduced about the minor axis. The columns were pin connected to the foundation. Two types

of beam-column connections exist in the CBF, one with gusset plates, the other without. For beam-column connections without the gusset plate, a spring with the force-deformation hysteretic model proposed by Liu and Astaneh-Asl [40] was used to model the rotational behaviour. The rotational hysteretic behaviour reported by Stoakes and Fahnestock [41] was adopted to define the rotational spring for the beam-gusset-column connection. The seismic masses (calculated based on the load combination 1.0D+0.25S) tributary to the studied CBF, i.e. placed on half of the plan view of the building, were applied at the top end of the two side columns. To account for the gravity loads and the vertical dynamic effect, the tributary gravity masses (calculated based on the load combination 1.0D+0.5L+0.25S) were applied at the top end of the three CBF columns, and a constant gravity acceleration was imposed throughout each dynamic analysis. Rayleigh damping of 2% was assigned to the first two modes of vibration of the structure.

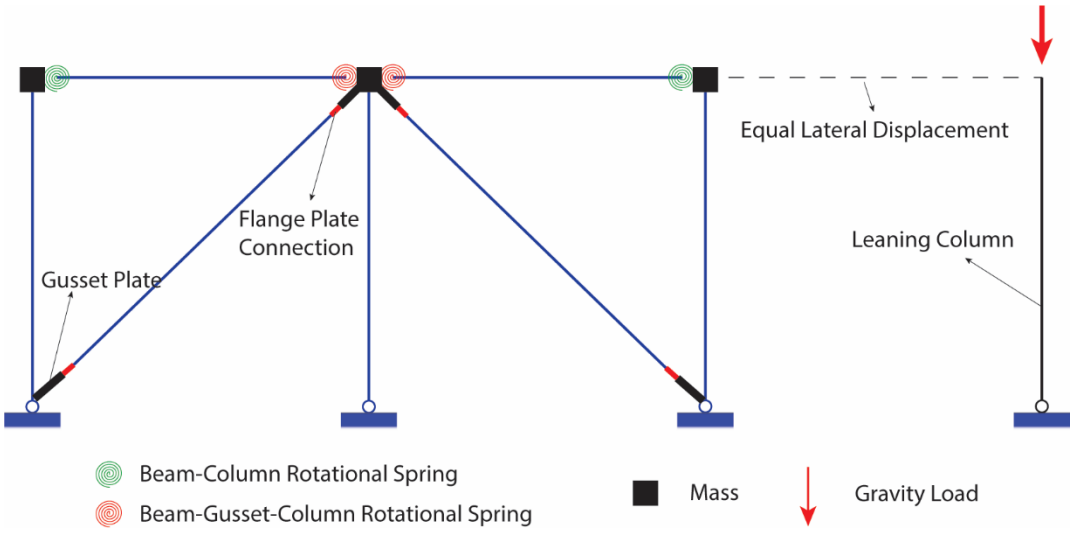

Figure 12 OpenSees model of CCBFs

In recognition of the lateral support for the beam provided by the steel roof deck or roof joists, beam deformations were confined to the CBF plane in the model. Moreover, to account for the

global P-delta effect, an elastic leaning column was incorporated in the model. The leaning column was pinned at the base and horizontally linked to the CBF at the roof level. The gravity load on half of the building (plan view), subtracting the portion directly resisted by the CBF, calculated based on the load combination 1.0D+0.5L+0.25S, was applied at the top of the leaning column throughout the analyses.

5 Nonlinear static analyses (Pushover)

The nonlinear static (Pushover) analyses of the archetype building CCBFs were first conducted to gain insight on the structural behaviour and limit state progression under seismic loading. All the CCBFs were pushed laterally at the roof level until significant lateral resistance loss. The base shear-storey drift curves are shown in Figure 13, with limit state progression marked along the loading process. The title of the sub-figure (e.g. “VE-EW”) corresponds to the first two parts of the CCBF ID listed in Table 2, and the legend (“100” or “150”) corresponds to the third part.

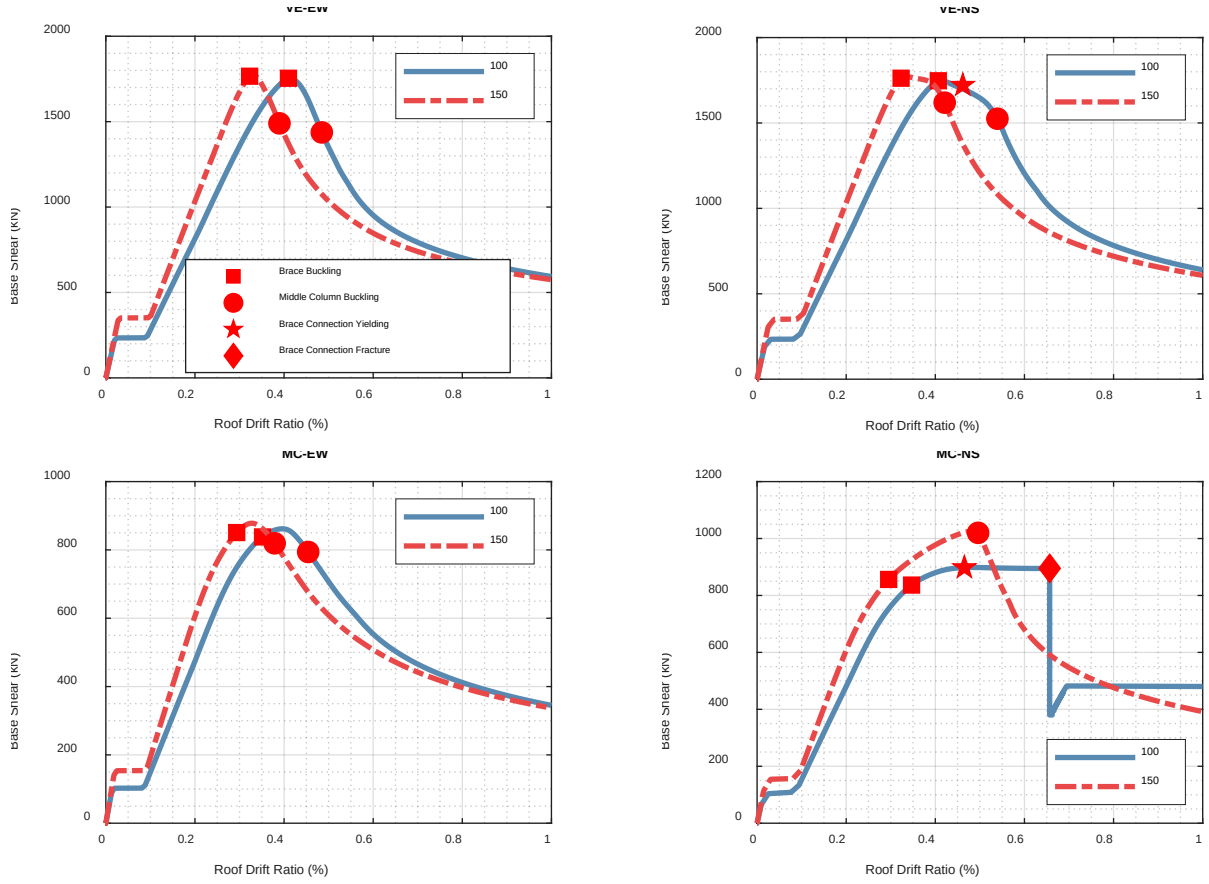

Figure 13 Roof drift-base shear curves of Pushover analyses

5.1 Limit state identification

The studied single-storey CCBFs followed similar limit state progression patterns to that shown in Figure 14. At the start of lateral loading, the two braces worked elastically (one in tension, the other in compression). As the lateral load increased, frictional slippage occurred in the bolted brace connections, resulting in a plateau in the base shear-storey drift curves. With increased lateral force, the compression brace buckled, resulting in a rapid and pronounced deterioration of its compressive strength. A significant unbalanced force was subsequently imposed on the middle column by the post-buckling force in the compression brace and the force in the adjacent tension brace. As the lateral drift increased, the force in the tension brace increased, as did the

unbalanced force on the middle column. Depending on the brace connection strength, yielding can occur in the tension brace connections at this stage. As the middle column was only designed to resist gravity loads, the unbalanced force triggered the buckling of the middle column in most cases, except for MC-NS-100. In the MC-NS-100 model, yielding concentrated in the tension brace connections, where fracture eventually occurred.

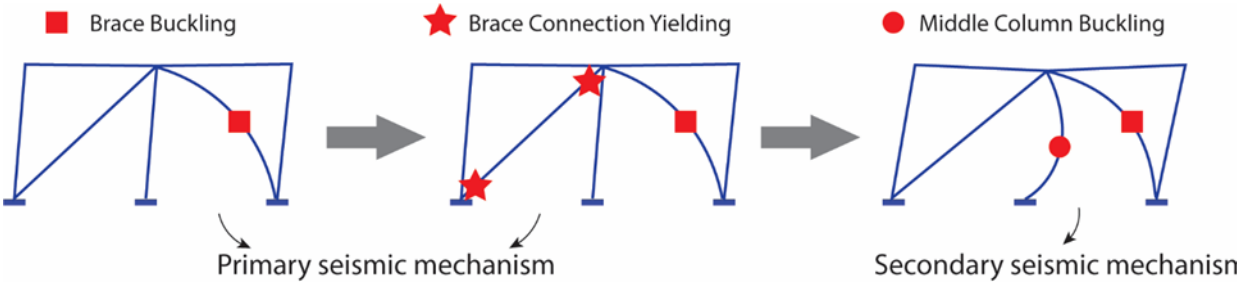

Figure 14 Progression of limit states to secondary seismic mechanism

After the middle column buckled, the lateral resistance of the studied CCBFs deteriorated substantially. However, as the lateral drift continued, the stable reserve lateral resistance was attained through the secondary seismic mechanism. In this mechanism, the tension brace and the adjoining column and beam worked as a rigid body, and the buckled brace and middle column provided support for the rigid body. Therefore, the failure of the local components may not result in the overall system failure of CCBFs, as secondary seismic mechanisms may form to provide lateral resistance. This phenomenon has also been demonstrated experimentally and numerically in previous studies on CCBFs by Simpson & Mahin [42] and Sizemore et al. [9].

5.2 Effect of brace connections

The plateaus in the base shear-storey drift curves in Figure 13 resulted from the frictional slippage in the bolted brace connections. Stronger brace connections resulted in connection slippage at higher frictional force levels, indicating the higher frictional energy-dissipating

capacity under cyclic loadings. After slippage occurred, the structures with stronger brace connections exhibited larger structural lateral stiffness and developed brace buckling at lower storey drifts compared to their counterparts with relatively weaker brace connections. In the case of MC-NS-100 (Figure 13), the yielding of the brace connection in tension resulted in a substantial loss in lateral stiffness of the structure, and notably affected the continued increase of lateral strength, as compared to MC-NS-150.

Moreover, stronger brace connections always triggered buckling of the middle column at smaller storey drifts. As explained by Wang et al. [12], the brace connection is the weakest compared to the adjoining brace and gusset plate in terms of tensile strength in CCBFs. As such, the brace connection determines the possible maximum force that is transferred by the braces to the middle column. After the compression brace buckles, a stronger brace connection imposes a larger unbalanced force on the middle column than a weaker brace connection at the same storey drift, which can trigger earlier middle column buckling.

5.3 Effect of beam orientation

Figure 13 shows that the CCBFs designed for buildings with the NS secondary beam orientation maintained their primary lateral resistance to larger storey drifts compared to the corresponding CCBFs of buildings with the EW secondary beam orientation. As discussed in Section 5.1, the buckling of the middle column resulted in significant structural lateral strength deterioration, which indicated the beginning of the secondary seismic mechanism. The stronger middle columns associated with the NS secondary beam orientation helped the structure maintain the primary seismic mechanism by delaying or eliminating buckling of the middle column.

6 Nonlinear response history analyses (NRHAs)

6.1 Selection and scaling of ground motion (GM) records

The ground motion (GM) records were selected and scaled to be representative of the seismotectonic environment and the geotechnical conditions at the location of the building. The selection and scaling were conducted following the guidelines provided in the NBCC [38], with reference to a target response spectrum corresponding to a probability of exceedance of 2% in 50 years (a return period of 2475 years). For buildings in Montreal, eleven GMs, divided into two suites (listed in Table 4) to cover the range of periods that contribute significantly to the seismic response of the building, were selected. Due to the absence of recorded GM data for this region of the country, simulated GM time histories were used [43]. For buildings in Vancouver, three suites of five GM records (listed in Table 5) were selected and scaled to represent the three seismic sources for this region—shallow crustal, subduction interface and subduction intra-slab earthquakes. The notation "S1G1" is used to denote GM 1 in suite 1, and so on. The mean response spectra of the individual suites and the corresponding targeted response spectra are shown in Figure 15.

Table 4 Ground motions for building in Montreal

ID.	Event Name	Magnitude	Distance (km)	Class Site	Scale Factor
S1G1	M6c2-1	6.0	24.8	C	1.55
S1G2	M6c1-1	6.0	17.0	C	0.80
S1G3	M6c2-1	6.0	25.6	C	1.49
S1G4	M6c2-8	6.0	26.1	C	1.78
S1G5	M6c2-1	6.0	25.6	C	1.51
S2G1	M7c2-4	7.0	50.3	C	1.63
S2G2	M7c2-1	7.0	47.8	C	1.50
S2G3	M7c2-6	7.0	62.6	C	2.15
S2G4	M7c2-8	7.0	69.9	C	1.92
S2G5	M7c2-3	7.0	45.2	C	0.93
S2G6	M7c2-1	7.0	41.6	C	1.19

Note: All the listed are simulated ground motion records from the source Engineering Seismology Toolbox of Canada (https://www.seismotoolbox.ca/index.html).

Table 5 Ground motions for building in Vancouver

ID.	Event Name	Magnitude	Record Station	Distance (km)	Class Site	Scale Factor
S1G1	Superstition Hills-02	6.5	Imperial Valley Wildlife Liquefaction Array	23.85	E	1.80
S1G2	Superstition Hills-02	6.5	Kornbloom Road (temp)	18.48	D	3.55
S1G3	Loma Prieta	6.9	Hollister Differential Array	24.82	D	1.70
S1G4	Darfield_ New Zealand	7.0	Christchurch Resthaven	19.48	E	1.50
S1G5	Victoria_ Mexico	6.3	Chihuahua	18.96	D	2.80
S2G1	Japan, Geiyo	6.8	IYO	47	D	1.94
S2G2	El Salvador,	7.7	San Miguel	109	D	3.76
S2G3	Japan, Geiyo	6.8	TOHWA	56	D	1.58
S2G4	El Salvador,	7.7	Armenia	90.48	E	0.81
S2G5	El Salvador,	7.7	Ahuachapán	137	D	2.26
S3G1	Japan, Tohoku	9.1	KYONAN	227	E	1.91
S3G2	Japan, Tohoku	9.1	MISAKI	190	E	2.13
S3G3	Japan, Tohoku	9.1	INAGE	179	D	1.99
S3G4	Japan, Tohoku	9.1	URAYASU	186	E	1.93
S3G5	Japan, Tohoku	9.1	TSUGAWA	203	D	3.29

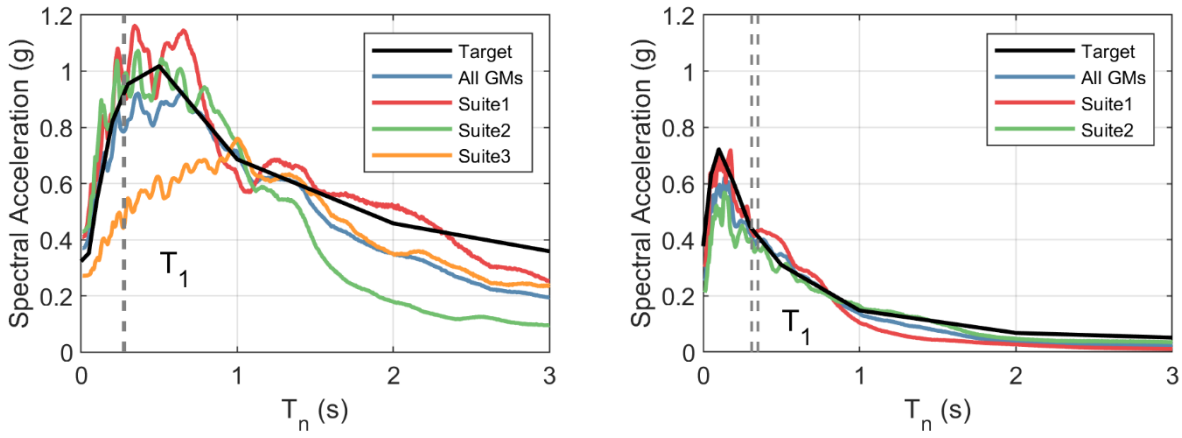

Figure 15 Mean response spectrum of GMs and target response spectrum: (a) Vancouver Site Class E; (b) Montreal Site Class C

6.2 Dynamic responses under selected ground motion

The nonlinear response history dynamic analyses showed that all buildings in Montreal exhibited low levels of maximum storey drifts and maintained their primary seismic mechanism under all selected GMs. In contrast, the CCBF systems for buildings in Vancouver developed the secondary seismic mechanism under some GMs. The responses of the VE-EW-100 and VE-EW-150 under GM S1G3 are representative of the seismic responses with the secondary seismic mechanism, which are shown in Figures 16 and 17, respectively. The storey drift response history, the base shear, and the response of each component were presented. It is noted that the axial deformation of the brace connection in Figures 16 and 17 referred to the total value of the two brace connections in one bay.

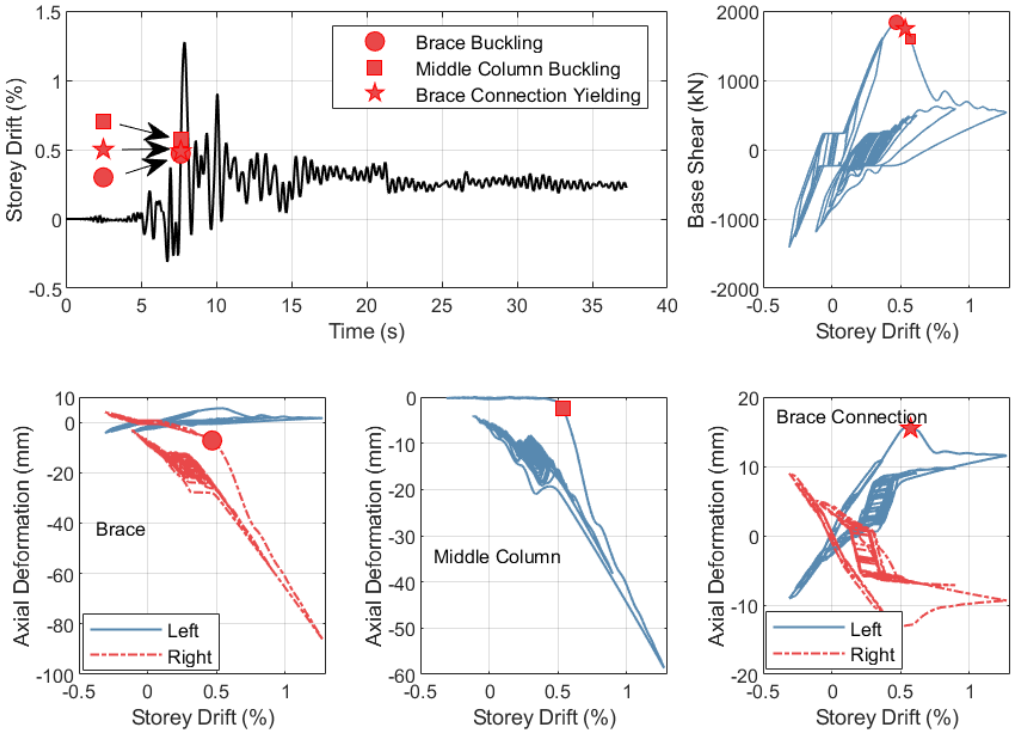

Figure 16 Seismic response of VE-EW-100 under S1G3

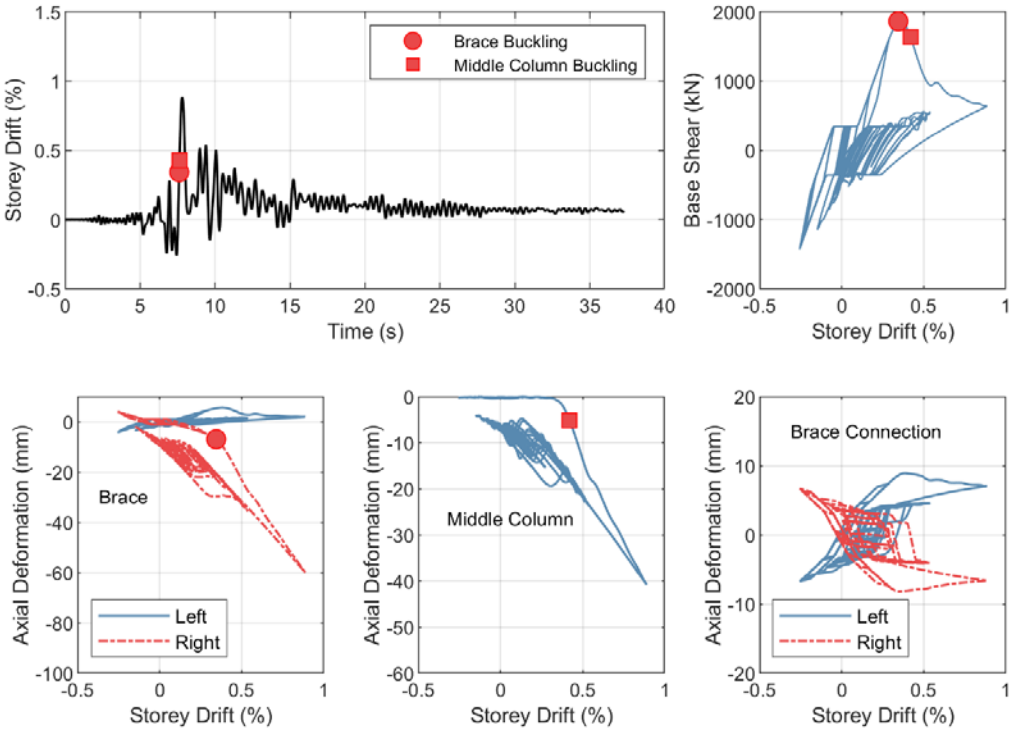

Figure 17 Seismic response of VE-EW-150 under S1G3

During the first 7.5 s of the GM shaking, both the CBFs remained elastic and cyclic frictional slippage occurred in the bolted brace connections. As the brace connection frictional resistance in VE-EW-150 is higher than in VE-EW-100, the plateaus in the base shear-storey drift curve were at higher base shear levels, which resulted in higher energy dissipation. Starting at the time of around 7.5 s, there was a large monotonic increase in the storey drift in the right direction. During this large storey drift excursion, the compression brace in the right bay buckled. As the storey drift increased further, the post-buckling resistance of the compression brace decreased and the force in the tension brace increased. As such, the axial compression force imposed on the middle column increased.

It is noted that before the middle column buckled, yielding occurred in the tension brace connections of the VE-EW-100. The maximum tensile deformation of the two brace connections in the left bay reached 15.6 mm, which was 2.82 times more than that of the tension brace, 5.5 mm. Even though all brace connections in the VE-EW-150 remained elastic throughout the analysis, the maximum tensile deformation of the two brace connections (8.9 mm) in the left bay was 1.56 times more than that of the brace (5.7 mm).

As the axial compression force increased, the middle columns in the two systems buckled. The base shear subsequently dropped substantially. However, structural instability did not occur as lateral resistance was provided through the secondary seismic mechanism, in which the unbuckled brace and the adjoining column and beam worked elastically as a rigid body, and the buckled brace and middle column provided support for the rigid body.

6.3 Maximum storey drift

The maximum storey drift ratios under individual GMs are plotted in Figure 18, with the mean value denoted by the dashed line for each CCBF. The CCBFs in Vancouver exhibited higher levels of maximum storey drifts than those in Montreal. For Vancouver, the maximum storey drifts were still quite low, with the maximum of 1.36% in VE-EW-100 under GM S1G3, compared to the NBCC limit of 2.5%. No structural instability occurred, indicating the satisfactory collapse-preventing performance of the single-storey CCBFs in both Montreal and Vancouver. Stronger brace connections led to smaller maximum storey drifts in most cases. This is believed to be attributed to the higher frictional energy-dissipation capacity of the stronger brace connections.

Compared with CCBFs with the EW secondary beam orientation, CCBFs designed with the NS secondary beam orientation exhibited lower maximum storey drifts. This is because stronger middle columns delayed the buckling of themselves and enabled the CCBF to maintain the primary lateral resistance until relatively larger storey drifts. The result indicated the potential of preventing middle column buckling for improved seismic performance of CCBFs with the studied bracing configuration, which could be attained by designing the middle column for the unbalanced brace forces. However, more direct analyses and evidence are needed to substantiate this design recommendation.

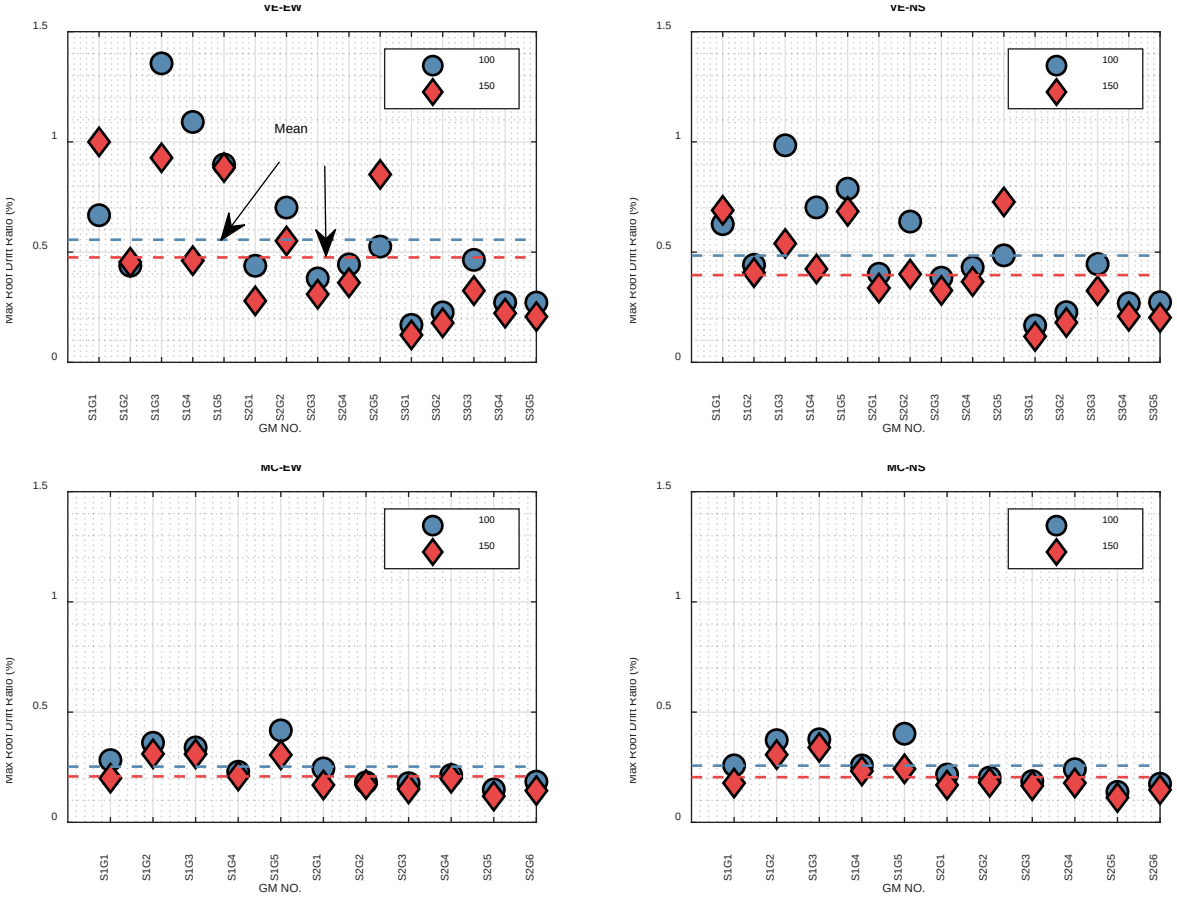

Figure 18 Maximum storey drifts

6.4 Brace connection deformation

As discussed in Section 6.1, when loaded in tension, the two brace connections contributed more deformation than the brace members themselves. Previous experimental studies [10,11] have witnessed the failure of brace connections designed for CCBFs. Therefore, the quantification of brace connection deformation demand is critical to establish the acceptance criteria for the brace connection ductility of CCBFs.

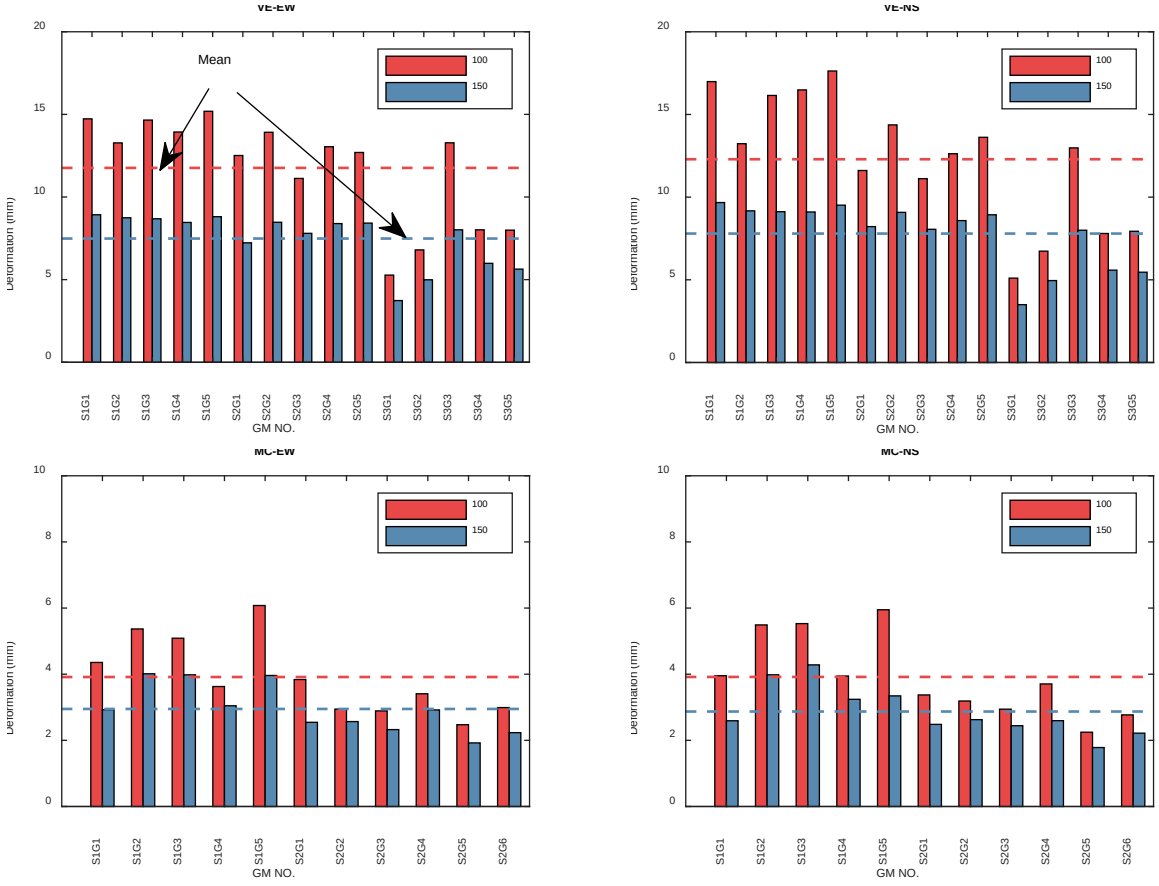

Figure 19 Maximum brace connection deformation

The maximum brace connection deformations under individual GMs are plotted in Figure 19. It is noted that the deformation amount is for only one brace connection. The brace connection deformation demands for CCBFs in Montreal were smaller than those of CCBFs in Vancouver,

indicating a lower demand of brace connection ductility for CCBFs in areas of lower seismic hazard.

Strengthening of the brace connections proved to be an effective way to reduce the deformation demand on the brace connections, which justified the seismic provision for brace connection design of CCBFs in the CSA S16 Standard [1]: “the seismic design force has to be amplified by 1.5 unless the brace connection is proved to be ductile”. The secondary beam orientation had a negligible effect on the brace connection deformation demand. Even though buildings with the NS secondary beam orientation exhibited lower levels of maximum storey drifts, the associated stronger middle column increased the tensile deformation demand by delaying the secondary seismic mechanism.

When interpreting the brace connection deformation demands presented in Figure 19, caution has to be taken as they were derived from the study on the single-storey CBFs with the symmetric diagonal bracing configuration with middle columns. Further studies are needed to quantify the brace connection deformation demand for CCBFs of different numbers of storeys and various bracing configurations, which is the topic of the ongoing research by the authors.

7 Conclusions

Brace connections in conventional CBFs (CCBFs) are expected to sustain inelastic deformations under strong earthquakes, and therefore, accurate numerical modelling of brace connections is critical for the reliable assessment of the seismic performance of CCBFs. In this paper, an efficient numerical model was proposed for the bolted flange plate brace connection by applying the component-based modelling method. The numerical model was validated to be able to

capture the brace connection force-deformation hysteretic behaviour and the onset of fracture with high accuracy.

Eight single-storey CCBFs with the symmetric diagonal bracing configuration were designed and analyzed. Through the nonlinear static analyses and nonlinear dynamic analyses, the main findings are:

1. The buckling of the middle column can result in significant lateral strength deterioration. However, the secondary seismic mechanism can provide stable remaining lateral resistance to prevent global structural instability.
2. When loaded in tension, the brace connections may deform (including the slippage) much more than the brace members themselves. The brace connection deformation demand is higher in areas of high seismic hazard. Strengthening brace connections is an effective way of reducing the deformation demand.
3. Stronger brace connections will lead to greater lateral stiffness of the structure and trigger earlier buckling of middle columns.
4. Stronger brace connections possess higher frictional energy-dissipating capacity, which can reduce the maximum storey drift.
5. Stronger middle columns will reduce the maximum storey drift, but have a negligible effect on the brace connection deformation demand.

It is noted that the conclusions are only applicable to the studied single-storey CCBFs with the symmetric diagonal bracing configuration. Further research is needed for CCBFs having different bracing configurations and a larger number of storeys.

Acknowledgements

The work was funded by the Natural Sciences and Engineering Research Council of Canada (NSERC), the Fonds de recherche du Québec-Nature et technologies (FRQ-NT) and the Centre d'études interuniversitaire des structures sous charges extremes (CEISCE). The financial and technical support from DPHV Structural Consultants and ADF Group Inc. is gratefully acknowledged. Assistance with the ground motion selection and scaling from Mr. Bashar Hariri at Polytechnique Montréal is greatly appreciated. The first author is supported in part through the China Scholarship Council (CSC). The numerical simulations were conducted on the supercomputer cluster Graham of Compute Canada, which is funded by the Canada Foundation for Innovation (CFI).

References

[1] Canadian Standards Association (CSA) S16-19. (2019). Design of steel structures. Toronto, ON, Canada.

[2] American Society of Civil Engineers/Structural Engineering Institute (ASCE/SEI) 7-16. (2016). Minimum Design Loads and associated criteria for buildings and other structures. Reston, Virginia, USA.

[3] EN 1998‐1. (2004). Eurocode 8: Design of Structures for Earthquake Resistance – Part 1: general Rules, Seismic Actions and Rules for Buildings. Brussels: European Committee for Standardization.

[4] Standards New Zealand (NZS). (2007). NZS 3404 Part 1:1997, Steel Structures Standard Incorporating Amendment No. 1 and Amendment No. 2., Wellington, NZ.

[5] Sen, A., Roeder, C., Lehman, D., Berman, J., Sloat, D., Ballard, R., & Johnson, M. (2016). Experimental evaluation of the seismic vulnerability of braces and connections in older concentrically braced frames. Journal of Structural Engineering, 142(9). doi:10.1061/(ASCE)ST.1943-541X.0001507

[6] Sen, A., Swatosh, M., Ballard, R., Sloat, D., Johnson, M., Roeder, C., Berman, J. (2017). Development and evaluation of seismic retrofit alternatives for older concentrically braced frames. Journal of Structural Engineering, 143(5), 04016232-04016232. doi:10.1061/(ASCE)ST.1943-541X.0001738

[7] Bradley, C., Fahnestock, L., Sizemore, J., & Hines, E. (2017). Full-scale cyclic testing of low-ductility concentrically braced frames. Journal of Structural Engineering, 143(6). doi:10.1061/(ASCE)ST.1943-541X.0001760

[8] Sizemore, J., Fahnestock, L., Hines, E., & Bradley, C. (2017). Parametric study of low-ductility concentrically braced frames under cyclic static loading. Journal of Structural Engineering, 20170601. doi:10.1061/(asce)st.1943-541x.0001761

[9] Sizemore, J., Fahnestock, L., & Hines, E. (2019). Seismic performance assessment of low-ductility concentrically braced frames. Journal of Structural Engineering, 145(4). doi:10.1061/(ASCE)ST.1943-541X.0002276

[10] Rudman, A., Tremblay, R., & Rogers, C. A. (2021). Conventional I-shape brace member bolted connections under seismic loading: Laboratory study. Journal of Constructional Steel Research, 184, 106795.

[11] Wang, C., González Ureña, A., Afifi, M., Rudman, A., Tremblay, R., Rogers, C. A. (2020) "Conventional construction steel braces with bearing plate energy dissipation", 17th World Conference on Earthquake Engineering, Sendai, Japan

[12] Wang, C., Rudman, A., Tremblay, R., Rogers, C.A. (2021). Numerical investigation into I-shape brace connections of conventional concentrically braced frames. Engineering Structures 236: 112091.

[13] Hsiao, P.-C., Lehman, D. E., & Roeder, C. W. (2012). Improved analytical model for special concentrically braced frames. Journal of Constructional Steel Research, 73, 80–94.

[14] Qu, B., Sanchez-Zamora, F., & Pollino, M. (2014). Mitigation of inter-story drift concentration in multi-story steel concentrically braced frames through implementation of rocking cores. Engineering structures, 70, 208-217.

[15] Qu, B., Sanchez-Zamora, F., & Pollino, M. (2015). Transforming seismic performance of deficient steel concentrically braced frames through implementation of rocking cores. Journal of Structural Engineering, 141(5), 04014139.

[16] Hsiao, P. C., Lehman, D. E., Berman, J. W., Roeder, C. W., & Powell, J. (2014). Seismic vulnerability of older braced frames. Journal of Performance of Constructed Facilities, 28(1), 108-120.

[17] Sen, A. D., Roeder, C. W., Lehman, D. E., & Berman, J. W. (2019). Nonlinear modeling of concentrically braced frames. Journal of Constructional Steel Research, 157, 103-120.

[18] Tremblay, R., & Davaran, A. (2020). Design of Bolted Single Shear Lap Connection with Different Thicknesses of Splice Plates. Journal of Structural Engineering, 146(3), 04020004.

[19] Shen, J., & Astaneh-Asl, A. (2000). Hysteresis model of bolted-angle connections. Journal of Constructional Steel Research, 54(3), 317–343. https://doi.org/10.1016/S0143-974X(99)00070-X

[20] Rassati, G. A., Noè S, & Leon, R. T. (2004). Component modeling of partially restrained composite joints under cyclic and dynamic loading. Journal of Structural Engineering, 130(2), 343–351. https://doi.org/10.1061/(ASCE)0733-9445(2004)130:2(343)

[21] Weigand, J. M. (2016). Component-based model for single-plate shear connections with pretension and pinched hysteresis. Journal of Structural Engineering, 143(2), 04016178–04016178.

[22] Rex, C. O., & Easterling, W. S. (2003). Behavior and modeling of a bolt bearing on a single plate. Journal of Structural Engineering, 129(6), 792-800. doi:10.1061/(asce)0733-9445(2003)129:6(792)

[23] Richard, R. M., & Abbott, B. J. (1975). Versatile elastic-plastic stress-strain formula. Journal of the Engineering Mechanics Division, 101(4), 511-515.

[24] Fisher, J. W., & Struik, J. H. A. (1974). Guide to design criteria for bolted and riveted joints. Wiley.

[25] Nelson, W. D., Bunin, B. L., & Hart-Smith, L. J. (1983). Critical joints in large composite aircraft structure (No. DP-7266). McDonnell Douglas Corp., Long Beach, CA.

[26] Weigand, J. M., & Berman, J. W. (2014). Integrity of steel single plate shear connections subjected to simulated column removal. Journal of Structural Engineering, 140(5), 04013114.

[27] Thomas, D. L., Wilson, J. M., & Wilson, R. R. (1973). Timoshenko beam finite elements. Journal of Sound and Vibration, 31(3), 315–330. https://doi.org/10.1016/S0022-460X(73)80276-7

[28] Weigand, J. M. (2014). The integrity of steel gravity framing system connections subjected to column removal loading. Ph.D. dissertation, Univ. of Washington, Seattle.

[29] Lesik, D. F., & Kennedy, D. J. L. (1990). Ultimate strength of fillet welded connections loaded in plane. Canadian Journal of Civil Engineering, 17(1), 55-67. doi:10.1139/l90-008

[30] McKenna, F., Fenves, G. L., Scott, M. H., & Jeremić, B. (2000). Open system for earthquake engineering simulation (http://opensees.berkeley.edu)

[31] Filippou, F. C., Popov, E. P., & Bertero, V. V. (1983). Effects of bond deterioration on hysteretic behavior of reinforced concrete joints. University of California Press, Berkeley, CA

[32] Wallaert, J. J., & Fisher, J. W. (1964). Shear strength of high-strength bolts. Fritz Laboratory Reports. 1822. https://preserve.lehigh.edu/engr-civil-environmental-fritz-lab-reports/1822

[33] Karamanci, E., & Lignos, D. G. (2014). Computational approach for collapse assessment of concentrically braced frames in seismic regions. Journal of Structural Engineering, 140(8), A4014019.

[34] Rudman, A. (2018). Testing of conventional construction W-shape brace members and their bolted end connections undergoing reversed cyclic loading. Master's thesis, Department of Civil Engineering, McGill University, Montreal, QC, Canada.

[35] Mazzoni, S., McKenna, F., Scott, M. H., and Fenves, G. L. (2006). OpenSees command language manual. Pacific Earthquake Engineering Research (PEER) Center, Berkeley, CA.

[36] Uriz, P., and Mahin, S. A. (2008). Toward earthquake-resistant design of concentrically braced steel-frame structures. PEER Rep. No. 2008/08, Univ. of California, Berkeley, Berkeley, CA.

[37] Wang, C., Tremblay, R., & Rogers, C. A. (2021). Parametric study on the I-shape brace connection of conventional concentrically braced frames. Journal of Constructional Steel Research, 182, 106669.

[38] National Research Council of Canada (NRCC). (2015). National Building Code of Canada (NBCC) (13th ed.). Ottawa, ON, Canada.

[39] American Institute of Steel Construction (AISC) 341-16. (2016). Seismic Provisions for Structural Steel Buildings. Chicago, IL: American Institute of Steel Construction.

[40] Liu, J., & Astaneh-Asl, A. (2004). Moment–rotation parameters for composite shear tab connections. Journal of Structural Engineering, 130(9), 1371–1380. https://doi.org/10.1061/(ASCE)0733-9445(2004)130:9(1371)

[41] Stoakes, C. D., & Fahnestock, L. A. (2011). Cyclic flexural testing of concentrically braced frame beam-column connections. Journal of Structural Engineering, 137(7), 739–747. https://doi.org/10.1061/(ASCE)ST.1943-541X.0000326

[42] Simpson, B. G., & Mahin, S. A. (2018). Experimental and numerical evaluation of older chevron concentrically braced frames with hollow and concrete-filled braces. Journal of Structural Engineering (United States), 146(1). https://doi.org/10.1061/(ASCE)ST.1943-541X.0001988

[43] Atkinson G. (2009). Earthquake time histories compatible with the 2005 NBCC uniform hazard spectrum. Canadian Journal of Civil Engineering, 36(6):991–1000.